STABILITY ANALYSIS OF INVERSE LAX-WENDROFF BOUNDARY TREATMENT OF HIGH ORDER COMPACT DIFFERENCE SCHEMES FOR PARABOLIC EQUATIONS

TINGTING LI, JIANFANG LU, AND CHI-WANG SHU

Abstract. In this paper, we study the stability of a numerical boundary treatment of high order compact finite difference methods for parabolic equations. The compact finite difference schemes could achieve very high order accuracy with relatively small stencils. To match the convergence order of the compact schemes in the interior domain, we take the simplified inverse Lax-Wendroff (SILW) procedure [24, 14] as our numerical boundary treatment. The third order total variation diminishing (TVD) Runge-Kutta method [18] is taken as our time-stepping method in the fully-discrete case. Two analysis techniques are adopted to check the algorithm's stability, one is based on the Godunov-Ryabenkii theory, and the other is the eigenvalue spectrum visualization method [26]. Both the semi-discrete and fully-discrete cases are investigated, and these two different analysis techniques yield consistent results. Several numerical experimental results are shown to validate the theoretical results.

1. Introduction

The finite difference approximations for derivatives are one of the simplest and oldest approaches to solve differential equations. To make a high order finite difference scheme work, one must take special treatment near the domain boundary, i.e. evaluating the numerical solution on the ghost points properly. As mentioned in [22], there exist two difficulties in obtaining high order accurate and stable numerical boundary conditions. One is the proper evaluation of the ghost point values located outside the computational domain which are used by the interior schemes. The other is that the grid points may not coincide with the physical boundary exactly, especially when a Cartesian mesh is used to solve problems on a complex geometry. There are many methods in the literature for handling boundary conditions on irregular domains, such as the body-fitted meshes [2, 8], the embedded boundary method [10, 21], the inverse Lax-Wendroff method (ILW) [22] and the simplified inverse Lax-Wendroff method (SILW) [4, 11, 12, 13, 14, 23, 24, 26] and so on. For these approaches, stability is a major concern especially when the

2010 *Mathematics Subject Classification.* 65M12.
Key words and phrases. high order compact difference schemes; parabolic equation; simplified inverse Lax-Wendroff procedure; Godunov-Ryabenkii theory; eigenvalue analysis.
T. Li's research is supported by NSFC grant 11801143.
J. Lu's research is partially supported by NSFC grant 11901213 and Guangdong Basic and Applied Basic Research Foundation 2020B1515310021.
C.-W. Shu's research is partially supported by NSF grant DMS-2010107 and AFOSR grant FA9550-20-1-0055.

cell intersects with the physical boundary, referred as the "cut-cell" problem. In finite volume methods, this leads to a restricted time step for the sake of stability, and the so-called h-box method is developed to overcome this difficulty, see [1] and the references therein. In this paper, we focus on the stability of the SILW procedure for high order compact finite difference schemes when solving diffusion problems. The SILW method uses Taylor expansion at the boundary point to get the approximation values on the ghost points. Derivatives at the boundary points are obtained by the ILW procedure and the interpolation polynomial, which will be explained in detail in later sections. There exists a vast variety of methods to get the interpolation polynomials. In the previous work [13, 14], the interpolation polynomial was obtained by the function values at the interior points and the boundary points. It would seem reasonable to expect the same method also works for the compact schemes. However, it turns out the extension is not so easy and we cannot find a stable scheme by the previous polynomial construction methods. To make it work, we choose the Birkhoff interpolation method to get the interpolation polynomials in this paper.

General stability analysis for initial boundary value problems (IBVP) on a bounded domain can be performed by the normal mode analysis, which is based on the Laplace transform. This method was firstly presented by Godunov and Ryabenkii [7] and then developed by Kreiss [9] and Osher [15]. The original Godunov-Ryabenkii theory only provided a necessary condition for stability. Later, Gustafsson, Kreiss and Sundström developed a necessary and sufficient condition for stability for the first order linear hyperbolic systems in one space dimension [5], which is referred to as the *GKS theory*. For parabolic problems, such stability analysis was formulated in, e.g. [16, 20, 25]. Later on, the semi-discrete case was studied by Strikwerda in [19]. Theoretically, the Godunov-Ryabenkii method leads to necessary conditions for stability, but in a vast number of cases they also appear to be sufficient conditions [20]. However, for high order schemes the Godunov-Ryabenkii method is not so advantageous due to the high algebraic complexity. In [26], the authors proposed an alternative technique by visualizing the eigenvalues spectrum of compact differencing operators, and they obtained consistent stability conclusions with the Godunov-Ryabenkii analysis. In our previous work [13, 14], both the GKS analysis and eigenvalue analysis were used to analyze stability of high order upwind-biased schemes for hyperbolic equations and high order central difference schemes for diffusion equations, and the two methods produced consistent stability conclusions. In this paper, we continue to extend the work to high order compact schemes for parabolic equations with Dirichlet or Neumann boundary conditions. The compact finite difference schemes are taken as our interior schemes, and the SILW

procedure is performed near the boundaries. With Godunov-Ryabenkii analysis and eigenvalue analysis, we report on the minimum number of spatial derivatives which must be obtained by the ILW procedure for the sake of stability for schemes of various order of accuracy. Although we only consider pure diffusion here, our eventual objective is to use the methodology for possibly convection dominated convection-diffusion equations, thus justifying the choice of explicit time-stepping methods throughout this paper.

This paper is organized as follows. In Sect. 2, we first give an overview of the discretization of the problem, that is, the high order compact finite difference schemes and the third order total variation diminishing (TVD) Runge-Kutta time discretization method used in the fully-discrete problems. The SILW procedure is introduced in detail in this section as well. In Sect. 3, stability analysis is performed both for the semi-discrete and fully-discrete cases by the Godunov-Ryabenkii method and the eigenvalue spectrum visualization method. In Sect. 4, numerical examples are given to demonstrate and validate the results of the analysis. Concluding remarks are given in Sect. 5.

2. Scheme formulation

In this section, we list the high order compact finite difference schemes used as the interior schemes considered in this paper. The third order explicit total variation diminishing (TVD) Runge-Kutta time discretization method [18] is used to get the fully-discrete schemes. We also give a detailed introduction of the SILW procedure for the boundary treatments.

2.1. **High order compact difference schemes.**

Consider the one-dimensional linear scalar heat equation

$$\begin{cases} u_t = c\, u_{xx}, \ x \in (a,b), \quad t > 0, \\ u(x,0) = u_0(x), \quad x \in (a,b), \end{cases} \tag{2.1}$$

with appropriate boundary conditions. For instance, we can take Dirichlet boundary conditions as

$$\begin{cases} u(a,t) = g_1(t), \ t \geq 0, \\ u(b,t) = g_2(t), \ t \geq 0, \end{cases} \tag{2.2}$$

or Neumann boundary conditions as

$$\begin{cases} u_x(a,t) = g_3(t), \ t \geq 0, \\ u_x(b,t) = g_4(t), \ t \geq 0, \end{cases} \tag{2.3}$$

or a suitable combination, where $c > 0$ is restricted by the well-posedness of the IBVP (2.1).

The interval (a,b) is discretized by a uniform mesh as

$$a + C_a\Delta x = x_0 < x_1 < x_2 < \cdots < x_N = b - C_b\Delta x \tag{2.4}$$

with the uniform mesh size $\Delta x = (b-a)/(C_a + C_b + N)$, $C_a, C_b \in [0,1)$. $\{x_j = a + (C_a + j)\,\Delta x,\ j = 0,1,2,\cdots N\}$ are the grid points. Note that the first and last points x_0 and x_N are not necessarily aligned with the boundary, and we choose this kind of discretization on purpose.

In [17], the authors presented the fourth order compact schemes for the discretization of u_{xx}, in which the stencil only consists of three points in the formula. Therefore, the scheme can be efficiently implemented by solving a tridiagonal matrix. Based on the low order compact schemes, we can derive the compact schemes for arbitrary even order in a uniform mesh.

The high order compact schemes considered in this paper are listed below.

• The fourth order scheme

CF1:

$$\frac{1}{12}(u_{xx})_{j-1} + \frac{5}{6}(u_{xx})_j + \frac{1}{12}(u_{xx})_{j+1} = \frac{1}{\Delta x^2}(u_{j-1} - 2u_j + u_{j+1})$$

• The sixth order schemes

CS1:

$$\begin{aligned}&\frac{2}{15}(u_{xx})_{j-1} + \frac{11}{15}(u_{xx})_j + \frac{2}{15}(u_{xx})_{j+1}\\ &\quad = \frac{1}{\Delta x^2}\Big(\frac{1}{20}u_{j-2} + \frac{4}{5}u_{j-1} - \frac{17}{10}u_j + \frac{4}{5}u_{j+1} + \frac{1}{20}u_{j+2}\Big)\end{aligned}$$

CS2:

$$\begin{aligned}&-\frac{1}{240}(u_{xx})_{j-2} + \frac{1}{10}(u_{xx})_{j-1} + \frac{97}{120}(u_{xx})_j + \frac{1}{10}(u_{xx})_{j+1} - \frac{1}{240}(u_{xx})_{j+2}\\ &\quad = \frac{1}{\Delta x^2}(u_{j+1} - 2u_j + u_{j-1})\end{aligned}$$

• The eighth order schemes

CE1:

$$\begin{aligned}&\frac{9}{56}(u_{xx})_{j-1} + \frac{19}{28}(u_{xx})_j + \frac{9}{56}(u_{xx})_{j+1} = \frac{1}{\Delta x^2}\Big(-\frac{23}{10080}u_{j-3} + \frac{51}{560}u_{j-2}\\ &\quad + \frac{21}{32}u_{j-1} - \frac{751}{504}u_j + \frac{21}{32}u_{j+1} + \frac{51}{560}u_{j+2} - \frac{23}{10080}u_{j+3}\Big)\end{aligned}$$

CE2:

$$\begin{aligned}&\frac{23}{3780}(u_{xx})_{j-2} + \frac{172}{945}(u_{xx})_{j-1} + \frac{131}{210}(u_{xx})_j + \frac{172}{945}(u_{xx})_{j+1} + \frac{23}{3780}(u_{xx})_{j+2}\\ &\quad = \frac{1}{\Delta x^2}\Big(\frac{31}{252}(u)_{j-2} + \frac{32}{63}u_{j-1} - \frac{53}{42}u_j + \frac{32}{63}u_{j+1} + \frac{31}{252}u_{j+2}\Big)\end{aligned}$$

CE3:

$$\frac{31}{60480}(u_{xx})_{j-3}-\frac{73}{10080}(u_{xx})_{j-2}+\frac{2171}{20160}(u_{xx})_{j-1}+\frac{12067}{15120}(u_{xx})_j \\ +\frac{2171}{20160}(u_{xx})_{j+1}-\frac{73}{10080}(u_{xx})_{j+2}+\frac{31}{60480}(u_{xx})_{j+3}=\frac{1}{\Delta x^2}(u_{j+1}-2u_j+u_{j-1})$$

- The tenth order schemes

CT1:

$$(u_{xx})_j=\frac{1}{\Delta x^2}\Big(\frac{1}{3150}u_{j-5}-\frac{5}{1008}u_{j-4}+\frac{5}{126}u_{j-3}-\frac{5}{21}u_{j-2}+\frac{5}{3}u_{j-1}-\frac{5269}{1800}u_j \\ +\frac{5}{3}u_{j+1}-\frac{5}{21}u_{j+2}+\frac{5}{126}u_{j+3}-\frac{5}{1008}u_{j+4}+\frac{1}{3150}u_{j+5}\Big)$$

CT2:

$$\frac{8}{45}(u_{xx})_{j-1}+\frac{29}{45}(u_{xx})_j+\frac{8}{45}(u_{xx})_{j+1} \\ =\frac{1}{\Delta x^2}\Big(\frac{43}{226800}u_{j-4}-\frac{74}{14175}u_{j-3}+\frac{247}{2025}u_{j-2}+\frac{1126}{2025}u_{j-1} \\ -\frac{4361}{3240}u_j+\frac{1126}{2025}u_{j+1}+\frac{247}{2025}u_{j+2}-\frac{74}{14175}u_{j+3}+\frac{43}{226800}u_{j+4}\Big)$$

CT3:

$$\frac{43}{3220}(u_{xx})_{j-2}+\frac{167}{805}(u_{xx})_{j-1}+\frac{899}{1610}(u_{xx})_j+\frac{167}{805}(u_{xx})_{j+1}+\frac{43}{3220}(u_{xx})_{j+2} \\ =\frac{1}{\Delta x^2}\Big(\frac{79}{28980}u_{j-3}+\frac{519}{3220}u_{j-2}+\frac{213}{644}u_{j-1}-\frac{2867}{2898}u_j+\frac{213}{644}u_{j+1} \\ +\frac{519}{3220}u_{j+2}+\frac{79}{28980}u_{j+3}\Big)$$

CT4:

$$-\frac{79}{585900}(u_{xx})_{j-3}+\frac{1873}{195300}(u_{xx})_{j-2}+\frac{7873}{39060}(u_{xx})_{j-1}+\frac{33863}{58590}(u_{xx})_j \\ +\frac{7873}{39060}(u_{xx})_{j+1}+\frac{1873}{195300}(u_{xx})_{j+2}-\frac{79}{585900}(u_{xx})_{j+3} \\ =\frac{1}{\Delta x^2}\Big(\frac{289}{1860}u_{j-2}+\frac{176}{465}u_{j-1}-\frac{331}{310}u_j+\frac{176}{465}u_{j+1}+\frac{289}{1860}u_{j+2}\Big)$$

CT5:

$$-\frac{289}{3628800}(u_{xx})_{j-4}+\frac{149}{129600}(u_{xx})_{j-3}-\frac{8593}{907200}(u_{xx})_{j-2}+\frac{101741}{907200}(u_{xx})_{j-1} \\ +\frac{57517}{72576}(u_{xx})_j+\frac{101741}{907200}(u_{xx})_{j+1}-\frac{8593}{907200}(u_{xx})_{j+2}+\frac{149}{129600}(u_{xx})_{j+3} \\ -\frac{289}{3628800}(u_{xx})_{j+4}=\frac{1}{\Delta x^2}(u_{j+1}-2u_j+u_{j-1})$$

In these formulas, u_j is the numerical approximation of the exact solution u at the grid point x_j, and $(u_{xx})_j$ is the numerical approximation of u_{xx} at x_j. Note that the tenth order scheme CT1 is not a compact scheme, it is a central difference scheme which

has already been analyzed in [14]. We put it here for comparison with other compact schemes. Then we obtain a semi-discrete interior scheme written as

$$U_t = \mathcal{L}(U)\,, \tag{2.5}$$

where $\mathcal{L}$ is discrete spatial operator.

2.2. **Time discretization.** For the fully-discrete scheme, we take the third order explicit total variation diminishing (TVD) Runge-Kutta method [18] as our time-stepping method to discretize (2.5) in time. We briefly introduce it below for clarity.

From the time level t_n to t_{n+1}, the third order TVD Runge-Kutta method is given by

$$\begin{aligned}
u^{(1)} &= u^n + \Delta t\mathcal{L}(u^n),\\
u^{(2)} &= \frac{3}{4}u^n + \frac{1}{4}u^{(1)} + \frac{1}{4}\Delta t\mathcal{L}(u^{(1)}),\\
u^{n+1} &= \frac{1}{3}u^n + \frac{2}{3}u^{(2)} + \frac{2}{3}\Delta t\mathcal{L}(u^{(2)}),
\end{aligned}$$

where Δt is the time step. Other types of time discretizations can also be analyzed along the same line.

To avoid order reduction, special attention must be paid when we impose time-dependent boundary conditions in the two intermediate stages of the Runge-Kutta method [3]. With the given boundary condition $g(t)$, the corresponding boundary conditions are given as follows.

$$\begin{aligned}
u^n &\sim g(t_n),\\
u^{(1)} &\sim g(t_n) + \Delta t g'(t_n),\\
u^{(2)} &\sim g(t_n) + \frac{1}{2}\Delta t g'(t_n) + \frac{1}{4}\Delta t^2 g''(t_n)\,.
\end{aligned}$$

2.3. **The simplified inverse Lax-Wendroff procedure.** The main idea of the inverse Lax-Wendroff procedure (ILW) is repeatedly using the partial differential equation (PDE) and boundary conditions to convert spatial derivatives to time and tangential derivatives of the given boundary condition. With these spatial derivatives, we then obtain the values of the ghost points by Taylor expansion. However, the algebra of the ILW procedure could be very heavy for fully nonlinear 2D systems. To overcome this difficulty, a simplified ILW method (SILW) was proposed in [24], with the ILW procedure to obtain the lower order spatial derivatives and extrapolation to obtain the higher order spatial derivatives. As the left and right boundaries are completely symmetric for parabolic equations with Dirichlet and Neumann boundary conditions, we will take the left boundary $x = a$ as an example to introduce the SILW procedure for (2.1) briefly.

2.3.1. *SILW procedure for Dirichlet boundary conditions.* In this subsection, we discuss the IBVP (2.1) with the boundary condition (2.2). Assume the inner approximation is a d-th order scheme. Taylor expansion at the boundary point $x = a$ is given as follows:

$$u(x_{-p}) = u(a + (C_a - p)\Delta x) = \sum_{k=0}^{d-1} \frac{u_a^{*(k)} \Delta x^k (-p + C_a)^k}{k!} + \mathcal{O}(\Delta x^d),$$

$$u_{xx}(x_{-p}) = u_{xx}(a + (C_a - p)\Delta x) = \sum_{k=0}^{d-3} \frac{u_a^{*(k+2)} \Delta x^k (-p + C_a)^k}{k!} + \mathcal{O}(\Delta x^{d-2})$$

where $u(x_{-p})$ is the value of the function u at the ghost points x_{-p} and $u_{xx}(x_{-p})$ is the value of the second order derivative u_{xx} at the ghost point x_{-p} respectively. Clearly, d-th order approximations of $u(x_{-p})$ and $(d-2)$-th order approximations of $u_{xx}(x_{-p})$ are

$$u_{-p} = \sum_{k=0}^{d-1} \frac{u_a^{*(k)} \Delta x^k (-p + C_a)^k}{k!}, \quad (u_{xx})_{-p} = \sum_{k=0}^{d-3} \frac{u_a^{*(k+2)} \Delta x^k (-p + C_a)^k}{k!} \tag{2.6}$$

where $u_a^{*(k)}$ is (at least) $(d-k)$-th order approximations of $\frac{\partial^k u}{\partial x^k}\Big|_{x=a}$. With the parabolic equation $u_t = c\, u_{xx}$ and the Dirichlet boundary conditions, we can use the PDE itself or extrapolation to get the even order derivatives, while the odd order derivatives can only be obtained by extrapolation. The details of the procedure are as follows.

- The even order derivatives can be obtained by the PDE itself through the inverse Lax-Wendroff (ILW) procedure:

$$u_a^{*(0)} = u(a,t) = g_1(t), \cdots, u_a^{*(2\beta)} = \frac{\partial^{(2\beta)} u}{\partial x^{(2\beta)}}\Big|_{x=a} = \frac{1}{c^\beta}\, g_1^{(\beta)}(t), \cdots$$

- All derivatives can be obtained by extrapolation.

Assume the d-th order scheme is used in the numerical approximation. We use the point values inside the computational domain to get the interpolation polynomial $P_{d-1}(x)$. Once $P_{d-1}(x)$ is obtained, then all derivatives can be obtained at the boundary with this interpolation polynomial. In [14], function values at the interior points and the boundary point are used to get $P_{d-1}(x)$ for the high order central difference schemes. However, for the compact difference schemes in this paper, we are not able to get a stable scheme by using the method in [14]. Instead, we use m point values of the function and $(d-m)$ point values of the second order partial derivative to get $P_{d-1}(x)$, which is a polynomial of degree $d-1$. That is, we use $\{(x_0, u_0), (x_1, u_1), \cdots, (x_{m-1}, u_{m-1}), (x_0, (u_{xx})_0), (x_1, (u_{xx})_1), \cdots, (x_{d-m-1}, (u_{xx})_{d-m-1})\}$ to get the interpolation polynomial $P_{l,d-1}(x)$. Here the subscript "l" stands for left. Then we have

$$u_a^{*(2\beta)} = \frac{\partial^{(2\beta)} u}{\partial x^{(2\beta)}}\Big|_{x=a} = P_{l,d-1}^{(2\beta)}(a), \quad u_a^{*(2\beta+1)} = \frac{\partial^{(2\beta+1)} u}{\partial x^{(2\beta+1)}}\Big|_{x=a} = P_{l,d-1}^{(2\beta+1)}(a).$$

The simplified inverse Lax-Wendroff (SILW) method is as follows. For $k_d = k_1$ ($1 \le k_1 \le d/2$), the even derivatives of $u_a^{*(2\beta)}$, $\beta = 0, 1, 2 \cdots k_1 - 1$ are obtained by the ILW procedure. The remaining derivatives in (2.6) are all obtained by extrapolation. In this way, we can get the values of the ghost points by Taylor expansion.

2.3.2. *SILW procedure for Neumann boundary conditions.* In this section, we discuss the IBVP (2.1) with the boundary condition (2.3). Assume the inner approximation is a d-th order scheme. Taylor expansion at the boundary point $x = a$ gives

$$u(x_{-p}) = u(a + (C_a - p)\Delta x) = \sum_{k=0}^{d} \frac{u_a^{*(k)} \Delta x^k (-p + C_a)^k}{k!} + \mathcal{O}(\Delta x^{d+1}),$$

$$u_{xx}(x_{-p}) = u_{xx}(a + (C_a - p)\Delta x) = \sum_{k=0}^{d-2} \frac{u_a^{*(k+2)} \Delta x^k (-p + C_a)^k}{k!} + \mathcal{O}(\Delta x^{d-1}).$$

where $u(x_{-p})$ is the value of the function u at the ghost points x_{-p}, $u_{xx}(x_{-p})$ is the value of the second order derivative u_{xx} at the ghost points x_{-p}, respectively. Similar as in [14], we also use $(d+1)$-th Taylor expansion to get the approximation values of the ghost points. Then we have u_{-p} and $(u_{xx})_{-p}$ as follows.

$$u_{-p} = \sum_{k=0}^{d} \frac{u_a^{*(k)} \Delta x^k (-p + C_a)^k}{k!}, \quad (u_{xx})_{-p} = \sum_{k=0}^{d-2} \frac{u_a^{*(k+2)} \Delta x^k (-p + C_a)^k}{k!}. \tag{2.7}$$

In the case of the parabolic equation $u_t = c\, u_{xx}$ with the Neumann boundary conditions, we can use the PDE itself or extrapolation to get the odd order derivatives, while the even order derivatives can only be obtained by extrapolation. The details of the procedure are as follows.

• The odd order derivatives can be obtained by the PDE itself through the inverse Lax-Wendroff (ILW) procedure:

$$u_a^{*(1)} = u_x(a,t) = g_3(t), \cdots, u_a^{*(2\beta+1)} = \frac{\partial^{(2\beta+1)} u}{\partial x^{(2\beta+1)}}\Big|_{x=a} = \frac{1}{c^\beta}\, g_3^{(\beta)}(t), \cdots$$

• All derivatives can be obtained by extrapolation.

Assume the d-th order scheme is used in the numerical approximation. As before, m point values of function and $(d + 1 - m)$ point values of the second order partial derivative are used to get the interpolation polynomial $P_d(x)$, which is a polynomial of degree d. We use $\{(x_0, u_0), \cdots, (x_{m-1}, u_{m-1}), (x_0, (u_{xx})_0), \cdots, (x_{d-m}, (u_{xx})_{d-m})\}$ to

get the interpolation polynomial $P_{l,d}(x)$. Then we have

$$u_a^{*(2\beta)} = \frac{\partial^{(2\beta)} u}{\partial x^{(2\beta)}}\Big|_{x=a} = P_{l,d}^{(2\beta)}(a), \quad u_a^{*(2\beta+1)} = \frac{\partial^{(2\beta+1)} u}{\partial x^{(2\beta+1)}}\Big|_{x=a} = P_{l,d}^{(2\beta+1)}(a).$$

The simplified inverse Lax-Wendroff (SILW) method is as follows. For $k_d = k_1$ $(1 \le k_1 \le d/2)$, the even derivatives of $u_a^{*(2\beta+1)}$, $\beta = 0, 1, 2 \cdots k_1 - 1$ are obtained by the ILW procedure. The remaining derivatives in (2.7) are obtained by extrapolation. In this way, we can get the values of the ghost points by Taylor expansion.

Clearly, a proper choice of k_d and m is the key point to ensure stability for numerical approximations of both Dirichlet and Neumann boundary conditions. Note that for the Dirichlet boundary, the possible value of m is $1, 2, \cdots, d$ and for the Neumann boundary condition, m can be choose as $1, 2, 3, \cdots, d+1$. We want to find the appropriate value of m and the corresponding minimum value of k_d that can ensure stability for all $C_a \in [0, 1)$. Notice that, the smaller the values of k_d, the simpler and less expensive the algorithm becomes. Hence we would like to find the smallest value of the the parameter k_d which can ensure stability.

3. Stability analysis

In this section, we consider the stability issue for both the semi-discrete and fully-discrete schemes. We apply the Godunov-Ryabenkii method and the eigenvalue spectrum visualization to analyze stability and these two methods yield similar results. The problem considered in this paper consists of two physical boundaries and each boundary can be analyzed separately, that is, stability can be discussed for two quarter-plane problems and a Cauchy problem. Furthermore, for the numerical approximation to the parabolic equation $u_t = c\, u_{xx}$, the left boundary and the right boundary are completely symmetric for a compact scheme. Therefore, we only perform stability analysis on the left boundary and we can obtain symmetric conclusions for the right boundary.

3.1. **Semi-discrete schemes.**

In this subsection, we discuss stability for the semi-discrete schemes. Stability is performed on the quarter-plane problem

$$\begin{cases} u_t = c\, u_{xx}, \ x \in [a, +\infty), \ t \ge 0, \\ u(a, t) = g_1(t), \ t \ge 0, \\ u(x, 0) = u_0(x), \ x \in [a, +\infty). \end{cases} \tag{3.8}$$

For convenience, we set $g_1(t) = 0$. Now let us take the fourth order scheme (3.9) as an illustration example.

$$\begin{cases} (u_j)_t = c\,(u_{xx})_j, \\ \dfrac{1}{12}(u_{xx})_{j-1} + \dfrac{5}{6}(u_{xx})_j + \dfrac{1}{12}(u_{xx})_{j+1} = \dfrac{1}{\Delta x^2}(u_{j-1} - 2u_j + u_{j+1}). \end{cases} \tag{3.9}$$

3.1.1. *Godunov-Ryabenkii stability analysis.* The key point of the Godunov-Ryabenkii method is to determine whether there exist any eigenvalues with positive real part. A complete description of the method can be found in [6, 19].

• Analysis on the Dirichlet boundary condition

For illustration purpose, we take $m = 4$, that is, the interpolation polynomial is obtained by $\{(x_0, u_0), (x_1, u_1), (x_2, u_2), (x_3, u_3)\}$.

Let $u_j = e^{st}\phi_j$, due to the fact that $u_t = c\,u_{xx}$, scheme (3.9) can be transformed into

$$\widetilde{s}\Big(\frac{1}{12}\phi_{j-1} + \frac{5}{6}\phi_j + \frac{1}{12}\phi_{j+1}\Big) = \phi_{j-1} - 2\phi_j + \phi_{j+1} \tag{3.10}$$

where $\widetilde{s} = s\Delta x^2/c$. $\widetilde{s}$ can also be regarded as eigenvalue and $\{\phi_j(\widetilde{s})\}_{j=0}^{\infty}$ is the corresponding eigensolution. For the fourth order scheme, the possible values of k_d are 1 and 2. Now we use $k_d = 1$ for instance.

Take $\phi_j = \kappa^j$ and plug it into equation (3.10), we can get the characteristic equation as follows.

$$\widetilde{s}\Big(\frac{1}{12} + \frac{5}{6}\kappa + \frac{1}{12}\kappa^2\Big) = \kappa^2 - 2\kappa + 1. \tag{3.11}$$

Define

$$f(\kappa) = \Big(1 - \frac{1}{12}\widetilde{s}\Big)\kappa^2 - \Big(2 + \frac{5}{6}\widetilde{s}\Big)\kappa + 1 - \frac{1}{12}\widetilde{s}\,. \tag{3.12}$$

Take $\kappa = e^{\imath\xi}$, $\xi \in [0, 2\pi]$, $|\kappa| = 1$. From (3.11), we can get

$$\widetilde{s} = \frac{12(\cos\xi - 1)}{\cos\xi + 5} \tag{3.13}$$

From (3.13), we can get $\widetilde{s}$ is real and $\widetilde{s} \le 0$ if $|\kappa| = 1$.

Since $x \in [a, +\infty)$, we are only interested in the roots of the characteristic equation satisfying $|\kappa| < 1$. Same as in [13], if $Re(\widetilde{s}) > 0$, equation (3.13) implies the number of roots for (3.11) with $|\kappa| < 1$ is independent of $\widetilde{s}$. We can take any value of $\widetilde{s}$ with $Re(\widetilde{s}) > 0$ and get the roots, then we can get the number of roots for (3.11) with $|\kappa| < 1$. Taking $\widetilde{s} = 1$, the roots of (3.12) are

$$\kappa_1 = 0.36714, \quad \kappa_2 = 2.72377.$$

Thus, there is only one root with $|\kappa| < 1$ when $Re(\widetilde{s}) > 0$. Then the general expression of ϕ_j in (3.10) is

$$\phi_j = \sigma\kappa^j. \tag{3.14}$$

For scheme (3.9), we need the ghost point values u_{-1} and $(u_{xx})_{-1}$. As $k_d = 1$, the derivatives are given as

$$
\begin{aligned}
u_a^{*(0)} &= u(a,t) = g_1(t) = 0,\\
u_a^{*(1)} &= \frac{1}{\Delta x}\big(-(3C_a^2+12C_a+11)u_0 + (9C_a^2+30C_a+18)u_1\\
&\quad -(9C_a^2+24C_a+9)u_2 + (3C_a^2+6C_a+2)u_3\big),\\
u_a^{*(2)} &= \frac{1}{\Delta x^2}\big((C_a+2)u_0 - (3C_a+5)u_1 + (3C_a+4)u_2 - (C_a+1)u_3\big),\\
u_a^{*(3)} &= \frac{1}{\Delta x^3}(-u_0+3u_1-3u_2+u_3).
\end{aligned}
\tag{3.15}
$$

Plugging (3.15) into (2.6) and we can get the approximate values at the ghost points

$$
\begin{aligned}
u_{-1} &= \frac{-C_a^2-6C_a^2-11C_a+18}{6}u_0 + \frac{C_a^3+5C_a^2+6Ca-12}{2}u_1\\
&\quad + \frac{-C_a^3-4C_a^2-3C_a+8}{2}u_2 + \frac{C_a^3+3C_a^2+2C_a-6}{6}u_3,\\
(u_{xx})_{-1} &= \frac{3u_0-8u_1+7u_2-2u_3}{\Delta x^2}.
\end{aligned}
\tag{3.16}
$$

Plugging (3.14) and (3.16) into (3.10) with $j = 0$ and we then have

$$
(a_3\kappa^3 + a_2\kappa^2 + a_1\kappa + a_0)\sigma = 0 \tag{3.17}
$$

where $a_0, \cdots, a_3$ are given as

$$
\begin{aligned}
a_0 &= \frac{2C_a^3+12C_a^2+22C_a+10\widetilde{s}-9}{12}, \quad a_1 = \frac{-6C_a^3-30C_a^2-36C_a+52+\widetilde{s}}{12},\\
a_2 &= \frac{6C_a^3+24C_a^2+18C_a-41}{12}, \quad a_3 = \frac{-C_a^3-3C_a^2-2C_a+5}{6}.
\end{aligned}
$$

In order to get a nontrivial ϕ_j, we need σ is nonzero and

$$
\begin{cases}
a_3\kappa^3 + a_2\kappa^2 + a_1\kappa + a_0 = 0,\\
f(\kappa) = 0,\\
|\kappa| < 1.
\end{cases}
\tag{3.18}
$$

For any $C_a \in [0,1)$, by solving equation (3.18) and taking the maximum value of $Re(\widetilde{s})$, we have the following result in Fig. 3.1.

The shaded region in Fig. 3.1 shows the maximum value of $Re(\tilde{s})$ for different C_a, the fact that the region is below $Re(\tilde{s}) = 0$ indicates stability. From Fig. 3.1, we can see all eigenvalues of the semi-discrete fourth order scheme CF1 satisfy $Re(\widetilde{s}) < 0$ for the Dirichlet boundary problem. This indicates the SILW procedure with $k_d = 1$ and $m = 4$ is stable for $C_a \in [0,1)$ and $C_b \in [0,1)$.

• Analysis on the Neumann boundary condition

Without loss of generality, we set $g_3(t) = 0$.

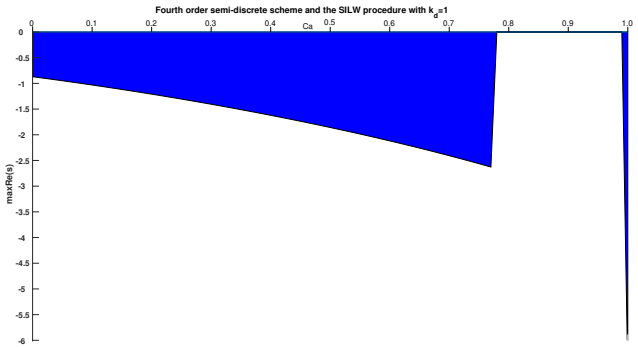

FIG. 3.1. Godunov-Ryabenkii stability analysis on the right-plane problem with Dirichlet boundary conditions: Fourth order semi-discrete scheme and SILW procedure with $k_d = 1$ and $m = 4$.

For the Neumann boundary condition, we need 5 points to get the interpolation polynomial. For illustration purpose, we choose $\{(x_0, u_0), (x_1, u_1), (x_2, u_2), (x_0, (u_{xx})_0), (x_1, (u_{xx})_1)\}$, i.e. $m = 3$. We also take $k_d = 1$.

As before, we have the characteristic equation is (3.11). The eigenvalue problem is (3.10) and the general expression of ϕ_j is (3.14). When $k_d = 1$, the values of derivatives are

$$
\begin{aligned}
u_a^{*(0)} &= \frac{C_a^4 + 2C_a^3 + C_a + 2}{2} u_0 + (-C_a^4 - 2C_a^3) u_1 + \frac{C_a^4 - C_a + 2C_a^3}{2} u_2 \\
&\quad + \frac{C_a^3 + 3C_a^2 + 2C_a}{6} \Delta x^2 (u_{xx})_0 + \frac{-3C_a^4 - 7C_a^3 + 4C_a}{6} \Delta x^2 (u_{xx})_1, \\
u_a^{*(1)} &= \frac{1}{c} g_3(t) = 0, \\
u_a^{*(2)} &= \frac{6C_a^2 + 6C_a}{\Delta x^2} u_0 - \frac{12C_a^2 + 12C_a}{\Delta x^2} u_1 + \frac{6C_a^2 + 6C_a}{\Delta x^2} u_2 \\
&\quad + (C_a + 1)(u_{xx})_0 + (-6C_a^2 - 7C_a)(u_{xx})_1, \\
u_a^{*(3)} &= \frac{-6(2C_a + 1)}{\Delta x^3} u_0 + \frac{12(2C_a + 1)}{\Delta x^3} u_1 - \frac{6(2C_a + 1)}{\Delta x^3} u_2 \\
&\quad - \frac{1}{\Delta x} (u_{xx})_0 + \frac{12C_a + 7}{\Delta x} (u_{xx})_1, \\
u_a^{*(4)} &= \frac{12u_0 - 24u_1 + 12u_2}{\Delta x^4} - \frac{12}{\Delta x^2} (u_{xx})_1.
\end{aligned}
\tag{3.19}
$$

Plugging (3.19) into (2.7) and we can get the approximate values at the ghost points

$$
\begin{aligned}
u_{-1} &= \Big(2C_a^4 + C_a^3 - 3C_a^2 + \frac{C_a}{2} + \frac{5}{2}\Big)u_0 + (-4C_a^4 - 2C_a^3 + 6C_a^2 - 3)u_1 \\
&\quad + \Big(2C_a^4 + C_a^3 - 3C_a^2 - \frac{C_a}{2} + \frac{3}{2}\Big)u_2 + \Big(\frac{C_a^3}{2} + \frac{C_a^2}{2} - \frac{2}{3}C_a + \frac{2}{3}\Big)\Delta x^2 (u_{xx})_0 \\
&\quad + \Big(-2C_a^4 - \frac{3}{2}C_a^3 + \frac{7}{2}C_a^2 + \frac{2}{3}C_a - \frac{5}{3}\Big)\Delta x^2 (u_{xx})_1, \\
(u_{xx})_{-1} &= \frac{12u_0 - 24u_1 + 12u_2}{\Delta x^2} + 2(u_{xx})_0 - 13(u_{xx})_1.
\end{aligned} \tag{3.20}
$$

Plugging (3.14) and (3.20) into (3.10) with $j = 0$ and we then have

$$
(b_2\kappa^2 + b_1\kappa + b_0)\sigma = 0 \tag{3.21}
$$

where b_0, b_1, b_2 are given as

$$
b_0 = -\frac{(C_a - 1)[12C_a^3 + 3(\widetilde{s} + 6)C_a^2 + 6\widetilde{s}C_a + 2\widetilde{s} + 3]}{6},
$$

$$
b_1 = \frac{(C_a - 1)[12(\widetilde{s} + 2)C_a^3 + 3(7\widetilde{s} + 12)C_a^2 - 4\widetilde{s}]}{6}, \quad b_2 = -\frac{(C_a - 1)(4C_a^3 + 6C_a^2 - 1)}{2}.
$$

In order to get a nontrivial ϕ_j, we need σ is nonzero and

$$
\begin{cases}
b_2\kappa^2 + b_1\kappa + b_0 = 0, \\
f(\kappa) = 0, \\
|\kappa| < 1.
\end{cases} \tag{3.22}
$$

For any $C_a \in [0, 1)$, by solving equation (3.22) and taking the maximum value of $Re(\widetilde{s})$ and we have the following result in Fig. 3.2.

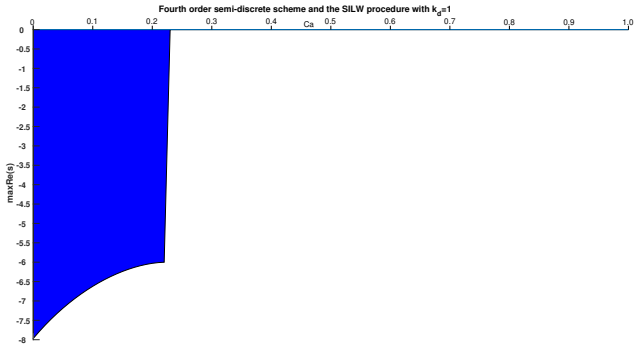

FIG. 3.2. Godunov-Ryabenkii analysis on the right-plane problem with Neumann boundary conditions: Fourth order semi-discrete scheme and SILW procedure with $k_d = 1$ and $m = 3$.

Fig. 3.2 indicates the semi-discrete fourth order scheme for the Neumann boundary problem with SILW procedure with $k_d = 1$ and $m = 3$ is stable for all $C_a \in [0, 1)$ and $C_b \in [0, 1)$.

3.1.2. *Eigenvalue spectrum visualization.* The algebra of the Godunov-Ryabenkii method is very complicated for the higher order schemes and we use an alternative eigenvalue spectrum visualization method which is easier to carry out to analyze stability. We will validate our analysis results by numerical experiments in the next section.

Unlike the Godunov-Ryabenkii method, which breaks the whole problem into three small problems, the method of eigenvalue spectrum visualization [26] needs to consider stability with the two boundaries together.

For simplicity, we set $g_1(t) = g_2(t) = g_3(t) = g_4(t) = 0$. The semi-discrete schemes can be transformed into a matrix-vector form as

$$\frac{d\vec{U}}{dt} = \frac{c}{\Delta x^2} Q\vec{U} \tag{3.23}$$

where $\vec{U} = (u_0, u_1, \cdots, u_N)^T$ and Q is a matrix. This system contains the chosen interior scheme and numerical boundary conditions.

Take $u(x,t) = e^{st}v(x)$ in (3.23) and it changes to

$$\tilde{s}\vec{U} = Q\vec{U} \tag{3.24}$$

As demonstrated in [26], stability has no relation with the grid number N, so we only need to focus on the eigenvalues which keep $O(1)$ distance from the imaginary axis when the grid number N increases and satisfy $Re(\tilde{s}) > 0$. Therefore, we look for "fixed" eigenvalues, namely those eigenvalues which are equal (subject to a negligible difference due to round-off errors and eigenvalue solver accuracy) for different values of grid number N. As in the case of the Godunov-Ryabenkii method, there may exist more than one "fixed" eigenvalue of the matrix Q, and we take the maximum value of the real part of the "fixed" eigenvalues. We also take the fourth order scheme (3.9) as an example to explain this method in detail.

Similar to the analysis in Sect. 3.1.1, we only analyze the stability of the right-plane problem. In order to get the matrix-vector form (3.23), we need a finite interval. For the fourth order scheme (3.9), the ghost points are u_{-1}, $(u_{xx})_{-1}$, u_{N+1} and $(u_{xx})_{N+1}$. As we are considering the right-plane problem, we get the ghost points u_{-1} and $(u_{xx})_{-1}$ by the SILW procedure and we set $u_{N+1} = (u_{xx})_{N+1} = 0$ to eliminate the influence to stability from the right boundary. In particular, for the Neumann boundary condition with $k_d = 1$, $m = 3$, we provide an explicit form of the matrix Q in details.

• Analysis on Dirichlet boundary condition

As before, we choose $k_d = 1$, $m = 4$ and use $\{(x_0, u_0), (x_1, u_1), (x_2, u_2), (x_3, u_3)\}$ to get the interpolation polynomial $P_{l,3}(x)$. We use different values of N to find the largest part of all the fixed eigenvalues, the result is in Fig. 3.3.

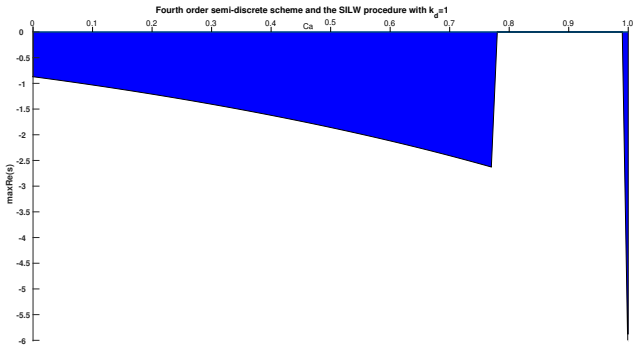

FIG. 3.3. Eigenvalue spectrum visualization on the right-plane problem with Dirichlet boundary conditions: Fourth order semi-discrete scheme and SILW procedure with $k_d = 1$ and $m = 4$.

From Fig. 3.1 and Fig. 3.3, we can see they are almost the same. So the eigenvalue spectrum visualization could be another approach to analyze stability.

• Analysis on the Neumann boundary condition

For the Neumann boundary condition, we choose $k_d = 1$, $m = 3$ and use $\{(x_0, u_0), (x_1, u_1), (x_2, u_2), (x_0, (u_{xx})_0), (x_1, (u_{xx})_1)\}$ to get $P_{l,4}(x)$. In this case, we have the numerical boundary condition (3.9) with $j = 0, N$ that

$$\begin{aligned} &\frac{1}{12}(u_{xx})_{-1} + \frac{5}{6}(u_{xx})_0 + \frac{1}{12}(u_{xx})_1 = \frac{1}{\Delta x^2}(u_{-1} - 2u_0 + u_1), \\ &\frac{1}{12}(u_{xx})_{N-1} + \frac{5}{6}(u_{xx})_N + \frac{1}{12}(u_{xx})_{N+1} = \frac{1}{\Delta x^2}(u_{N-1} - 2u_N + u_{N+1}), \end{aligned} \tag{3.25}$$

where the ghost points u_{-1} and $(u_{xx})_{-1}$ are obtained by the SILW procedure in (3.20) and we take $u_{N+1} = (u_{xx})_{N+1} = 0$. Then (3.25) can be rewritten as follows:

$$\begin{aligned} &m_0(u_{xx})_0 + m_1(u_{xx})_1 = \frac{1}{\Delta x^2}(n_0u_0 + n_1u_1 + n_2u_2), \\ &\frac{1}{12}(u_{xx})_{N-1} + \frac{5}{6}(u_{xx})_N = \frac{1}{\Delta x^2}(u_{N-1} - 2u_N), \end{aligned} \tag{3.26}$$

with m_0, m_1, n_0, n_1, n_2 are given as

$$\begin{aligned} m_0 &= \frac{2 + 4C_a - 3C_a^2 - 3C_a^3}{6}, \quad m_1 = \frac{4 - 4C_a - 21C_a^2 + 9C_a^3 + 12C_a^4}{6}, \\ n_0 &= \frac{-1 + C_a - 6C_a^2 + 2C_a^3 + 4C_a^4}{2}, \quad n_1 = 2C_a^2(3 - C_a - 2C_a^2), \\ n_2 &= \frac{1 - C_a - 6C_a^2 + 2C_a^3 + 4C_a^4}{2}. \end{aligned}$$

The fourth order scheme (3.9) then can be transformed into $M\frac{d^2\vec{U}}{dx^2} = \frac{1}{\Delta x^2}N\vec{U}$ with

$$M = \begin{pmatrix} m_0 & m_1 & & & & & \\ \frac{1}{12} & \frac{5}{6} & \frac{1}{12} & & & & \\ & \ddots & \ddots & \ddots & & & \\ & & \ddots & \ddots & \ddots & & \\ & & & \frac{1}{12} & \frac{5}{6} & \frac{1}{12} & \\ & & & & \frac{1}{12} & \frac{5}{6} & \end{pmatrix}, \quad N = \begin{pmatrix} n_0 & n_1 & n_2 & & & & \\ 1 & -2 & 1 & & & & \\ & \ddots & \ddots & \ddots & & & \\ & & \ddots & \ddots & \ddots & & \\ & & & 1 & -2 & 1 & \\ & & & & 1 & -2 & \end{pmatrix}.$$

Due to the fact that $\frac{d\vec{U}}{dt} = c\frac{d^2\vec{U}}{dx^2}$, we can rewrite the fourth order scheme in the form of (3.23) with $Q = M^{-1}N$. For different values of C_a, by analyzing the "fixed" eigenvalues of Q, we can get the result in Fig. 3.4.

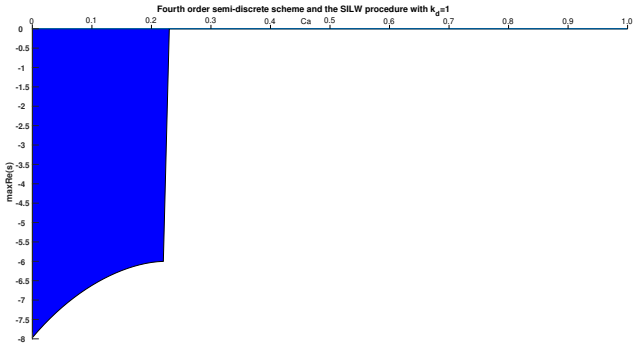

FIG. 3.4. Eigenvalue spectrum visualization on the right-plane problem with Neumann boundary conditions: Fourth order semi-discrete scheme and SILW procedure with $k_d = 1$ and $m = 3$.

3.2. **Fully-discrete Schemes.** In this paper, we use the third order TVD Runge-Kutta method as the time discretization method for scheme (3.9). The detailed procedure can be found in [13].

In the semi-discrete case, an eigensolution is in the form $u_j(t) = e^{st}\phi_j = e^{\tilde{s}c\frac{t}{\Delta x^2}}\phi_j$ with $Re(\widetilde{s}) > 0$. Analogously, in the fully-discrete scheme an eigensolution is in the form $u_j^{n+1} = z(\mu)u_j^n$ with $\mu = s\Delta t = \tilde{s}\lambda_{cfl}$, $\lambda_{cfl} = \dfrac{c\Delta t}{\Delta x^2}$ and $|z(\mu)| > 1$ where

$$z(\mu) = 1 + \mu + \frac{\mu^2}{2} + \frac{\mu^3}{6}. \tag{3.27}$$

Here, $\tilde{s}$ is an eigenvalue of the semi-discrete scheme and $z(\mu)$ is the eigenvalue of the fully-discrete scheme. In both semi-discrete and fully-discrete cases, the scheme is unstable if such candidate eigensolution exists.

Before studying the stability of the schemes for the initial-boundary value problem considered in this paper, we need to fix the CFL number first. Here we consider the CFL

condition of the numerical schemes for the corresponding Cauchy problem. We can get the maximum value of λ_{cfl}, denoted as $(\lambda_{cfl})_{max}$, which ensures stability of the schemes without boundary (periodic boundary conditions). Throughout this paper, we adopt $(\lambda_{cfl})_{max}$ as our CFL number when verifying the stability of the numerical schemes for the initial-boundary value problem. This means we do not want the boundary treatment to affect the CFL number of interior schemes for the corresponding Cauchy problem. The detailed procedure to find $(\lambda_{cfl})_{max}$ can be found in [13] and we just list the values of $(\lambda_{cfl})_{max}$ for the schemes in Sect. 2.1 in Table 3.1.

TABLE 3.1. $(\lambda_{cfl})_{\max}$ for schemes of different schemes

Scheme	CF1	CS1	CS2	CE1	CE2	CE3	CT1	CT2	CT3	CT4	CT5
$(\lambda_{cfl})_{max}$	0.418	0.366	0.376	0.343	0.336	0.356	0.368	0.329	0.320	0.322	0.343

3.2.1. *Godunov-Ryabenkii stability analysis.* For the Godunov-Ryabenkii stability analysis, $\tilde{s}$ is the eigenvalue obtained in the semi-discrete case and

$$\mu = s\Delta t = (\lambda_{cfl})_{max}\tilde{s}.$$

• Dirichlet boundary condition

As in Sect. 3.1.1, there may exist more than one eigenvalue $\tilde{s}$, hence there may exist more than one eigenvalue $z(\mu)$. The maximum value of $|z(\mu)|$ defined in equation (3.27) is shown in Fig. 3.5.

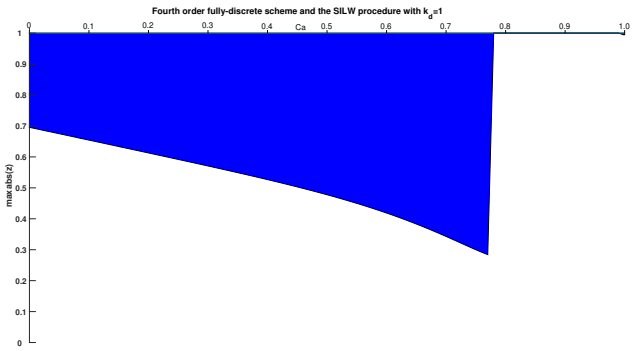

FIG. 3.5. Godunov-Ryabenkii analysis on the right-plane problem with Dirichlet boundary conditions: Fourth order fully-discrete scheme and SILW procedure with $k_d = 1$ and $m = 4$.

The shaded region in Fig. 3.5 shows the the maximum value of $|z(\mu)|$ for different C_a, the fact that the region is above $|z(\mu)| = 1$ indicates instability.

• Neumann boundary condition

The result for the Neumann boundary condition is shown in Fig. 3.6.

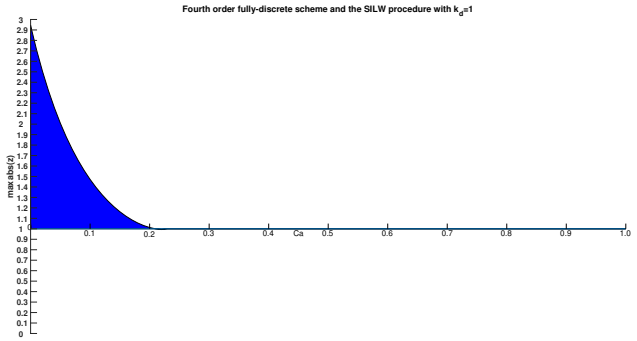

FIG. 3.6. Godunov-Ryabenkii analysis on the right-plane problem with Neumann boundary conditions: Fourth order fully-discrete scheme and SILW procedure with $k_d = 1$ and $m = 3$.

3.2.2. *Eigenvalue spectrum visualization.* In this subsection, we use the eigenvalue spectrum visualization method to get the stability results for the fully-discrete scheme. This method is based on the matrix formulation (3.23). By using the third order TVD Runge-Kutta method, we can get the fully-discrete scheme

$$\vec{U}^{n+1} = \Big(I + \frac{c\Delta t}{\Delta x^2}Q + \frac{1}{2}\Big(\frac{c\Delta t}{\Delta x^2}Q\Big)^2 + \frac{1}{6}\Big(\frac{c\Delta t}{\Delta x^2}Q\Big)^3\Big)\vec{U}^n \tag{3.28}$$

where I is the identity matrix. Same as in [13], we need all the eigenvalues of

$$G = I + \frac{c\Delta t}{\Delta x^2}Q + \frac{1}{2}\Big(\frac{c\Delta t}{\Delta x^2}Q\Big)^2 + \frac{1}{6}\Big(\frac{c\Delta t}{\Delta x^2}Q\Big)^3$$

to lie inside the unit circle. i.e. $|z(\mu)| \leq 1$, to ensure stability of the fully-discrete approximation.

- Dirichlet boundary condition

The maximum value of $|z(\mu)|$ as defined in equation (3.27) is shown in Fig. 3.7.

- Neumann boundary condition

The result of the Neumann boundary value problem is in Fig. 3.8.

Comparing Fig. 3.5 with Fig. 3.7, we can see that Fig. 3.5 is similar to Fig. 3.7 and Fig. 3.6 is similar to Fig. 3.8, which indicates these two methods yield the same results.

In conclusion, for the Dirichlet boundary value problem, the fully-discrete fourth order scheme and SILW procedure with $k_d = 1$ and $m = 4$ is stable for all $C_a \in [0, 1)$ and $C_b \in [0, 1)$. For the Neumann boundary value problem, the fully-discrete fourth order scheme and SILW procedure with $k_d = 1$ and $m = 3$ is stable for $C_a \in [0.21, 1)$ and $C_b \in [0.21, 1)$. In the later section, we will show that we need to take $k_d = 2$ to get a stable scheme for all $C_a \in [0, 1)$ and $C_b \in [0, 1)$.

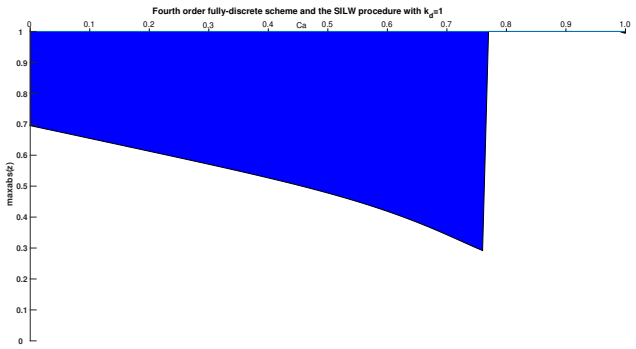

FIG. 3.7. Eigenvalue spectrum visualization on the right-plane problem with Dirichlet boundary conditions: Fourth order fully-discrete scheme and SILW procedure with $k_d = 1$ and $m = 4$.

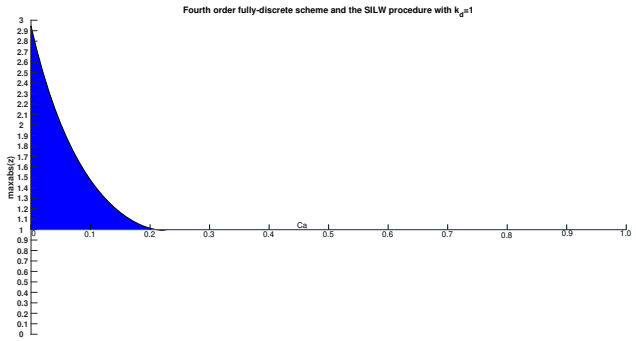

FIG. 3.8. Eigenvalue spectrum visualization on the right-plane problem with Neumann boundary conditions: Fourth order fully-discrete scheme and SILW procedure with $k_d = 1$ and $m = 3$.

For the remaining schemes in Sect. 2.1, we have obtained similar results. Suppose the interior scheme is d-th order, for the Dirichlet boundary value problem, m can be chosen as $1, \cdots, d$; for the Neumann boundary value problem, m can be chosen as $1, \cdots, d+1$. For every possible value of m, we would like to find the minimum value of k_d denoted as $(k_d)_{min}$ to guarantee stability for all $C_a \in [0, 1)$ and $C_b \in [0, 1)$. It maybe more than one pair of $(m, (k_d)_{min})$ that can get the stable results. In Table 3.2, we summarize all possible pairs of $(m, (k_d)_{min})$ to ensure stability of different schemes for the IBVP (2.1) with the Dirichlet boundary conditions (2.2), under the CFL conditions shown in Table 3.1. Results for the IBVP (2.1) with the Neumann boundary conditions (2.3) are shown in Table 3.3.

TABLE 3.2. Pairs of $(m, (k_d)_{min})$ to ensure stability for different schemes for IBVP (2.1) with Dirichlet boundary conditions (2.2).

Scheme	Pairs of $(m, (k_d)_{min})$
CF1	(4,1)
CS1	(6,2)
CS2	(6,2)
CE1	(3,3), (6,3), (8,2)
CE2	(3,3), (5,3), (6,3)
CE3	(3,3), (6,3), (8,2)
CT1	(2,2), (3,3), (4,4), (6,4), (7,3), (8,3), (9,2)
CT2	(3,3),(4,3),(6,3), (7,3), (8,3)
CT3	(3,3), (4,3), (6,3), (7,3), (8,3)
CT4	(3,3), (4,3), (6,3), (7,3), (8,3)
CT5	(3,3), (4,3), (7,3), (8,3), (10,2)

4. Numerical Example

In this section, we present some numerical examples to illustrate and validate the results in Tables 3.2 and 3.3. These numerical tests also indicate the obtained stability results are sufficient for stability of the boundary treatments.

Consider the following problem

$$\begin{cases} u_t = u_{xx}, \ x \in (1.5, 3.5), \ t \geq 0 \\ u(x,0) = \sin(x), \ x \in (1.5, 3.5). \end{cases} \tag{4.29}$$

The corresponding Dirichlet boundary conditions are

$$\begin{cases} u(1.5,t) = e^{-t}\sin(1.5), \\ u(3.5,t) = e^{-t}\sin(3.5). \end{cases} \tag{4.30}$$

The corresponding Neumann boundary conditions are

$$\begin{cases} u_x(1.5,t) = e^{-t}\cos(1.5), \\ u_x(3.5,t) = e^{-t}\cos(3.5). \end{cases} \tag{4.31}$$

The exact solution is

$$u(x,t) = e^{-t}\sin(x)$$

TABLE 3.3. Pairs of $(m, (k_d)_{min})$ to ensure stability for different schemes for IBVP (2.1) with Neumann boundary conditions (2.3).

Scheme	Pairs of $(m, (k_d)_{min})$
CF1	(2,2), (3,2)
CS1	(2,2), (6,2), (7,1)
CS2	(2,2), (6,2)
CE1	(2,2), (8,2)
CE2	(2,3), (8,2)
CE3	(2,2), (8,2), (9,2)
CT1	(3,3), (9,3)
CT2	(2,4), (10,3)
CT3	(6,4)
CT4	(10,4)
CT5	(2,3), (10,3), (11,2)

The time step size Δt is chosen as

$$\Delta t = (\lambda_{cfl})_{max} \Delta x^2 \tag{4.32}$$

and $(\lambda_{cfl})_{max}$ is the maximum CFL number shown in Table 3.1.

4.1. **Results for Dirichlet Boundary Condition.** In this subsection, we show the numerical results of boundary treatments for equation (4.29) with the boundary condition (4.30).

• The fourth order scheme

Here $m = 4$ and $(k_d)_{min} = 1$. Table 4.4 shows that we can get the fourth order with small and large C_a and C_b.

• The sixth order scheme CS1

In this case, $m = 6$ and the minimum value of k_d is $(k_d)_{min} = 2$. The left figure in Fig. 4.9 shows the scheme is unstable with $k_d = 1$. The right figure in Fig. 4.9 and Table 4.5 indicate the scheme is stable with $k_d = 2$, and we can see clearly sixth convergence order in Table 4.5.

• The sixth order scheme CS2

TABLE 4.4. The fourth order scheme CF1 with $m = 4$, $k_d = 1$, $t_{end} = 1.0$ for the heat equation (4.29) with Dirichlet boundary conditions (4.30). The CFL condition is in (4.32).

N	$C_a = 10^{-8}$, $C_b = 10^{-8}$				$C_a = 1 - 10^{-8}$, $C_b = 1 - 10^{-8}$			
	L^2 *error*	order	L^∞ *error*	order	L^2 *error*	order	L^∞ *error*	order
10	4.218E-04	–	4.382E-04	–	6.030E-05	–	6.700E-05	–
20	2.473E-05	4.092	2.779E-05	3.979	5.211E-06	3.533	6.040E-06	3.472
40	1.488E-06	4.054	1.740E-06	3.998	3.861E-07	3.754	4.567E-07	3.725
80	9.116E-08	4.029	1.087E-07	4.001	2.636E-08	3.873	3.151E-08	3.857
160	5.638E-09	4.015	6.787E-09	4.001	1.724E-09	3.935	2.071E-09	3.928

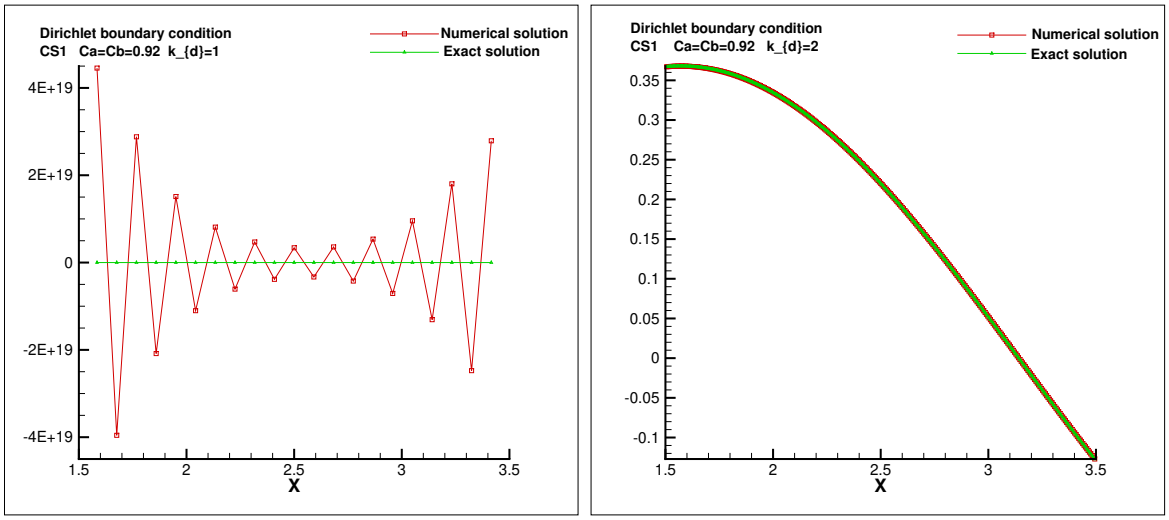

FIG. 4.9. The sixth order scheme CS1 and SILW procedure with $m = 6$, $C_a = C_b = 0.92$, $t_{end} = 1.0$. The CFL condition is in (4.32). Left: $k_d = 1$ and $N = 20$; Right: $k_d = 2$ and $N = 320$.

TABLE 4.5. The sixth order scheme CS1 with $m = 6$, $k_d = 2$, $t_{end} = 1.0$ for the heat equation (4.29) with Dirichlet boundary conditions (4.30). The CFL condition is in (4.32).

N	$C_a = 10^{-8}$, $C_b = 10^{-8}$				$C_a = 1 - 10^{-8}$, $C_b = 1 - 10^{-8}$			
	L^2 *error*	order	L^∞ *error*	order	L^2 *error*	order	L^∞ *error*	order
10	7.084E-06	–	6.731E-06	–	1.514E-06	–	1.572E-06	–
20	1.015E-07	6.125	1.091E-07	5.947	3.777E-08	5.325	4.383E-08	5.164
40	1.504E-09	6.076	1.722E-09	5.985	7.517E-10	5.651	9.210E-10	5.573
80	2.284E-11	6.041	2.698E-11	5.996	1.330E-11	5.821	1.671E-11	5.785
160	3.516E-13	6.021	4.220E-13	5.999	2.213E-13	5.909	2.813E-13	5.892

From previous analysis, we can get that $m = 6$ and $(k_d)_{min} = 2$. Fig. 4.10 shows the stable and unstable results and Table 4.6 shows the sixth order when the scheme is stable.

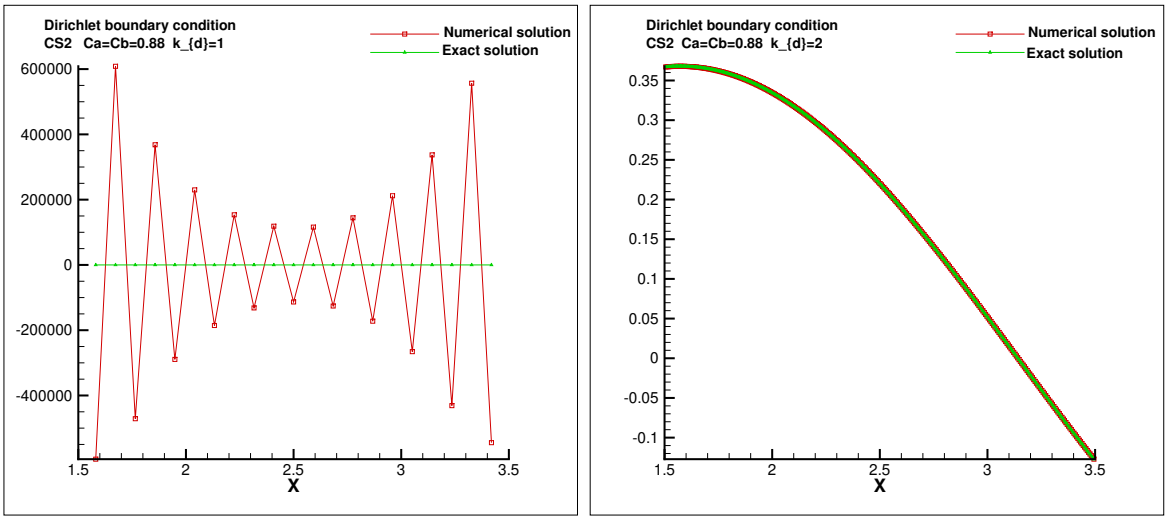

FIG. 4.10. The sixth order scheme CS2 and SILW procedure with $m = 6$, $C_a = C_b = 0.88$, $t_{end} = 1.0$. The CFL condition is in (4.32). Left: $k_d = 1$ and $N = 20$; Right: $k_d = 2$ and $N = 320$.

TABLE 4.6. The sixth order scheme CS2 with $m = 6$, $k_d = 2$, $t_{end} = 1.0$ for the heat equation (4.29) with Dirichlet boundary conditions (4.30). The CFL condition is in (4.32).

N	$C_a = 10^{-8}$, $C_b = 10^{-8}$				$C_a = 1 - 10^{-8}$, $C_b = 1 - 10^{-8}$			
	L^2 *error*	order	L^∞ *error*	order	L^2 *error*	order	L^∞ *error*	order
10	6.842E-06	–	6.491E-06	–	2.850E-07	–	2.938E-07	–
20	9.812E-08	6.124	1.053E-07	5.946	7.193E-09	5.308	8.144E-09	5.173
40	1.455E-09	6.076	1.662E-09	5.985	1.444E-10	5.638	1.710E-10	5.573
80	2.210E-11	6.041	2.605E-11	5.996	2.568E-12	5.814	3.104E-12	5.784
160	3.403E-13	6.021	4.074E-13	5.999	4.286E-14	5.905	5.229E-14	5.892

• The eighth order scheme CE1

We only explore the case with $m = 3$ and $(k_d)_{min} = 3$. Stability and instability results are given in Fig. 4.11. The results are consistent with the analysis.

• The eighth order scheme CE2

In this case, we only give the results with $m = 5$ and the corresponding $(k_d)_{min}$ is 3. Fig. 4.12 gives the stability and instability results.

• The eighth order scheme CE3

Here, we take $m = 6$ and $(k_d)_{min} = 3$. Stability and instability results are shown in Fig. 4.13.

• The tenth order scheme CT1

Fig. 4.14 gives the results with $m = 4$ and $(k_d)_{min} = 4$ and the results are consistent with the analysis before.

• The tenth order scheme CT2

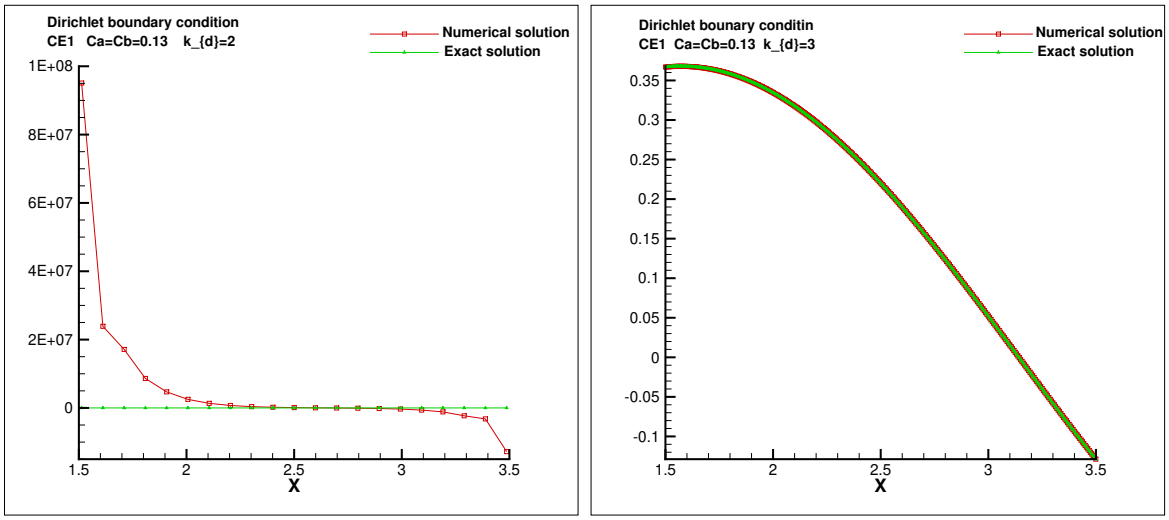

FIG. 4.11. The eighth order scheme CE1 and SILW procedure with $m = 3$, $C_a = C_b = 0.13$, $t_{end} = 1.0$. The CFL condition is in (4.32). Left: $k_d = 2$ and $N = 20$; Right: $k_d = 3$ and $N = 320$.

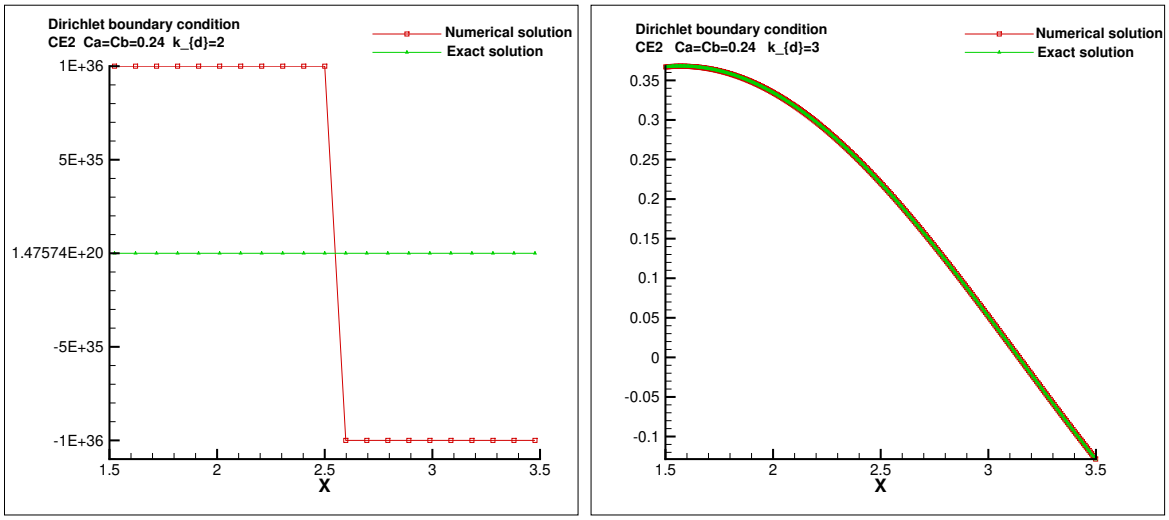

FIG. 4.12. The eighth order scheme CE2 and SILW procedure with $m = 5$, $C_a = C_b = 0.24$, $t_{end} = 1.0$. The CFL condition is in (4.32). Left: $k_d = 2$ and $N = 20$; Right: $k_d = 3$ and $N = 320$.

Fig. 4.15 is the stability and instability results of $m = 6$ and we can get that $(k_d)_{min} = 3$ and this is consistent with the stability analysis.

• The tenth order scheme CT3

In this case, we take $m = 3$ and $(k_d)_{min} = 3$. Stability and instability results are given in Fig. 4.16. The results are again consistent with the analysis.

• The tenth order scheme CT4

We give the numerical results with $m = 7$ and $(k_d)_{min} = 3$. Fig. 4.17 shows the stability and instability results.

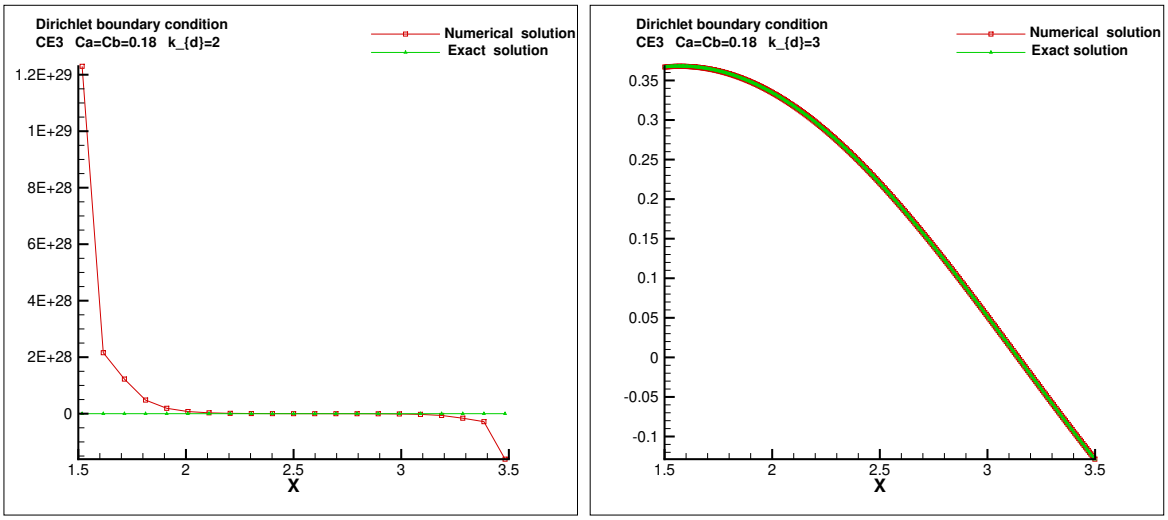

FIG. 4.13. The eighth order scheme CE3 and SILW procedure with $m = 6$, $C_a = C_b = 0.18$, $t_{end} = 1.0$. The CFL condition is in (4.32). Left: $k_d = 2$ and $N = 20$; Right: $k_d = 3$ and $N = 320$.

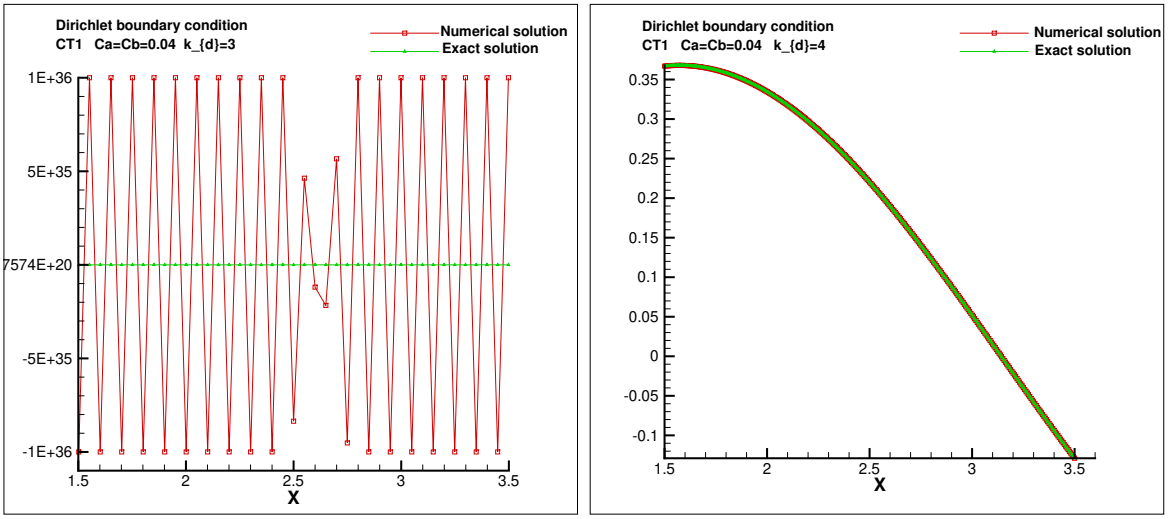

FIG. 4.14. The tenth order scheme CT1 and SILW procedure with $m = 4$, $C_a = C_b = 0.04$, $t_{end} = 1.0$. The CFL condition is in (4.32). Left: $k_d = 3$ and $N = 40$; Right: $k_d = 4$ and $N = 320$.

• The tenth order scheme CT5

In this case, we only display the results with $m = 8$ and $(k_d)_{min} = 3$. Fig. 4.18 shows the stability and instability results.

4.1.1. *Results for Neumann Boundary Condition.* In this subsection, we give the results of equation (4.29) with the boundary condition (4.31).

• The fourth order scheme CF1

Here, we only explore the case with $m = 3$. From previous discussion, if $k_d = 1$ the scheme is stable for $C_a \in [0.21, 1)$ and $C_b \in [0.21, 1)$. The left figure in Fig. 4.19 shows the

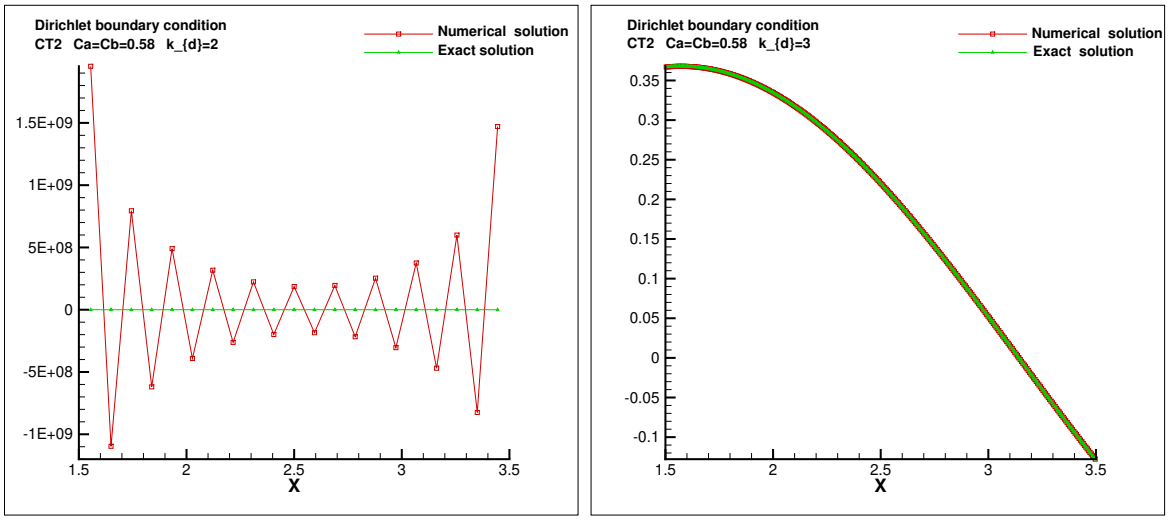

FIG. 4.15. The tenth order scheme CT2 and SILW procedure with $m = 6$, $C_a = C_b = 0.58$, $t_{end} = 1.0$. The CFL condition is in (4.32). Left: $k_d = 2$ and $N = 20$; Right: $k_d = 3$ and $N = 320$.

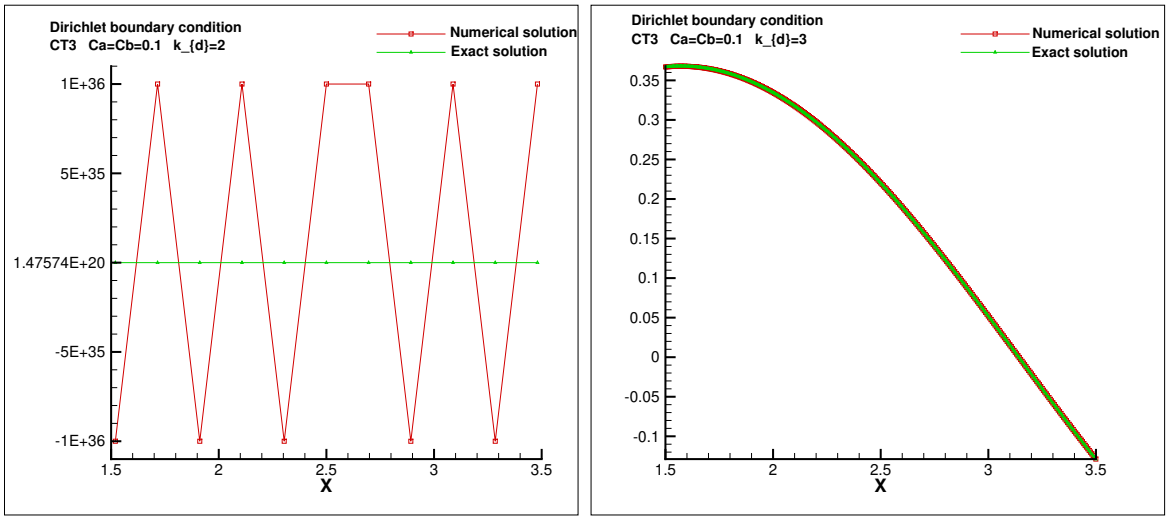

FIG. 4.16. The tenth order scheme CT3 and SILW procedure with $m = 3$, $C_a = C_b = 0.1$, $t_{end} = 1.0$. The CFL condition is in (4.32). Left: $k_d = 2$ and $N = 10$; Right: $k_d = 3$ and $N = 320$.

solution has strong spurious oscillations with very large magnitudes if $C_a = C_b = 0.2$ and the right one shows that the solution remains stable and accurate after grid refinements if $C_a = C_b = 0.21$. The numerical result confirm the theoretical results from the stability analysis. From Table 4.7, a grid refinement study verifies the designed fourth order accuracy when $k_d = 2$, which can ensure stability for $C_a \in [0, 1)$ and $C_b \in [0, 1)$.

- The sixth order scheme CS1

Here, we take $m = 6$ as an illustration example. In this case, $(k_d)_{min} = 2$ is the minimum value to ensure stability for all $C_a \in [0, 1)$ and $C_b \in [0, 1)$. The left figure in

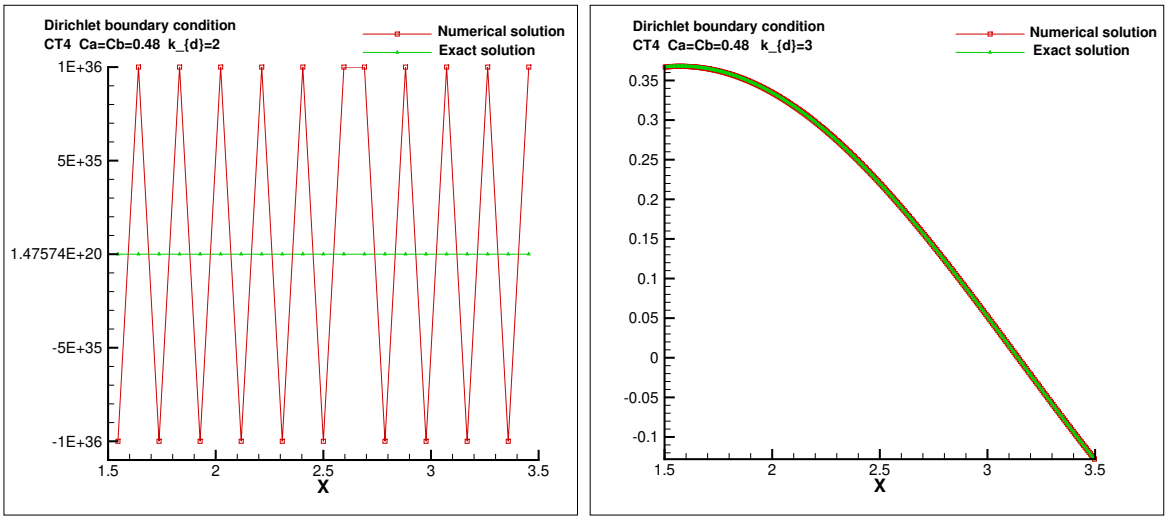

FIG. 4.17. The tenth order scheme CT4 and SILW procedure with $m = 7$, $C_a = C_b = 0.48$, $t_{end} = 1.0$. The CFL condition is in (4.32). Left: $k_d = 2$ and $N = 20$; Right: $k_d = 3$ and $N = 320$.

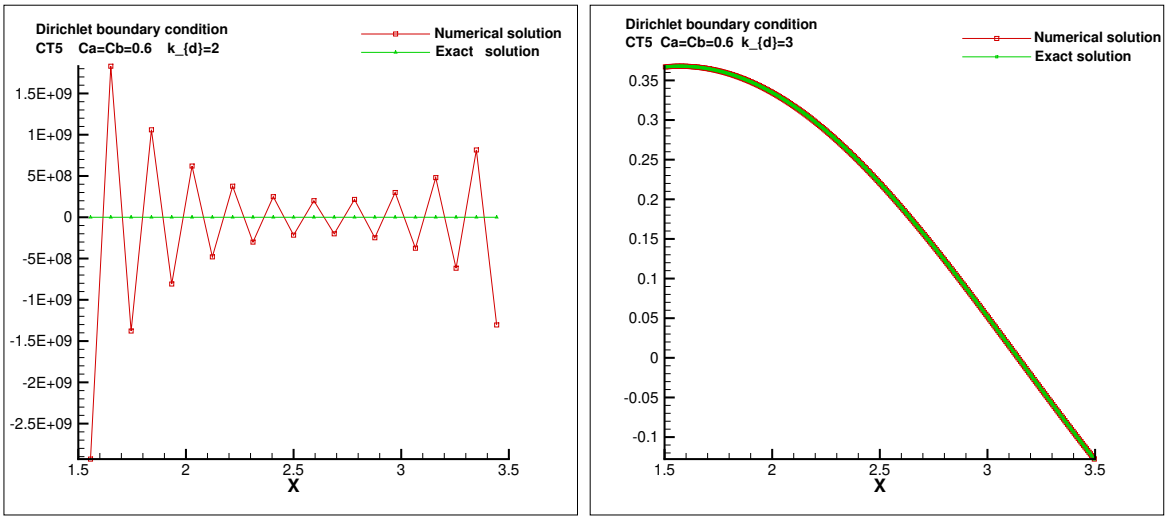

FIG. 4.18. The tenth order Scheme CT5 and SILW procedure with $m = 8$, $C_a = C_b = 0.6$, $t_{end} = 1.0$. The CFL condition is in (4.32). Left: $k_d = 2$ and $N = 20$; Right: $k_d = 3$ and $N = 320$.

Fig. 4.20 clearly shows instability and the right one shows stability. Table 4.8 shows the optimal convergence order.

• The sixth order scheme CS2

In this case, we also only give the results of $m = 6$. In order to get a stable scheme for all $C_a \in [0, 1)$ and $C_b \in [0, 1)$, we should take $(k_d)_{min} = 2$. Fig. 4.21 gives the stable and unstable results with $k_d = 1$ and $k_d = 2$. Table 4.9 gives the results with $k_d = 2$ after grid refinements. Theoretically, for the sixth order scheme and the third order Runge-Kutta method under the CFL condition (4.32), we are supposed to get a

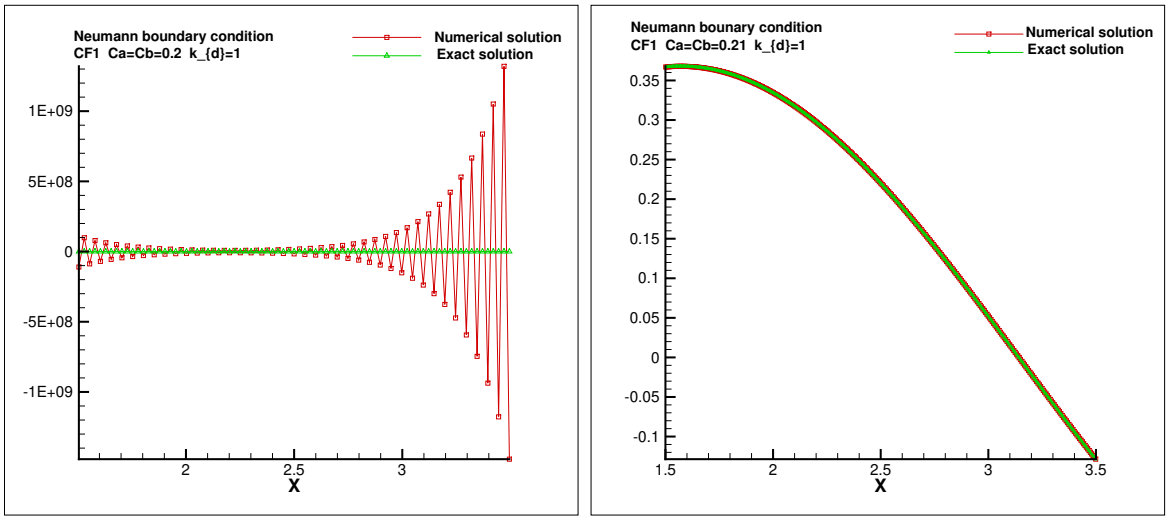

FIG. 4.19. The fourth order scheme CF1 and SILW procedure with $m = 3$, $k_d = 1$, $t_{end} = 1.0$. The CFL condition is in (4.32). Left: $C_a = C_b = 0.2$ and $N = 80$; Right: $C_a = C_b = 0.21$ and $N = 320$.

TABLE 4.7. The fourth order scheme CF1 with $m = 3$, $k_d = 2$, $t_{end} = 1.0$ for the heat equation (4.29) with Neumann boundary conditions (4.31). The CFL condition is in (4.32).

N	$C_a = 10^{-8}$, $C_b = 10^{-8}$				$C_a = 1 - 10^{-8}$, $C_b = 1 - 10^{-8}$			
	L^2 *error*	order	L^∞ *error*	order	L^2 *error*	order	L^∞ *error*	order
10	2.835E-06	–	3.889E-06	–	5.943E-05	–	7.867E-05	–
20	1.664E-07	4.091	2.416E-07	4.008	5.840E-06	3.347	7.483E-06	3.394
40	1.007E-08	4.046	1.507E-08	4.003	4.633E-07	3.656	5.805E-07	3.688
80	6.192E-10	4.023	9.412E-10	4.001	3.273E-08	3.823	4.048E-08	3.842
160	3.839E-11	4.012	5.882E-11	4.000	2.176E-09	3.910	2.673E-09	3.921

TABLE 4.8. The Sixth order scheme CS1 with $m = 6$, $k_d = 2$, $t_{end} = 1.0$ for the heat equation (4.29) with Neumann boundary conditions (4.31). The CFL condition is in (4.32).

N	$C_a = 10^{-8}$, $C_b = 10^{-8}$				$C_a = 1 - 10^{-8}$, $C_b = 1 - 10^{-8}$			
	L^2 *error*	order	L^∞ *error*	order	L^2 *error*	order	L^∞ *error*	order
10	4.762E-08	–	5.321E-08	–	5.919E-06	–	8.188E-06	–
20	5.846E-10	6.348	6.467E-10	6.363	1.829E-07	5.016	2.407E-07	5.088
40	8.135E-12	6.167	8.933E-12	6.178	4.079E-09	5.486	5.171E-09	5.541
80	1.202E-13	6.080	1.318E-13	6.082	7.642E-11	5.738	9.472E-11	5.771
160	1.808E-15	6.055	1.975E-15	6.060	1.308E-12	5.868	1.602E-12	5.886

sixth order scheme, but we can only obtain the fourth order numerically when C_a and C_b are large. Therefore we increase the number of interpolation points to get higher order interpolation polynomial and then we can obtain the desired sixth order. To be

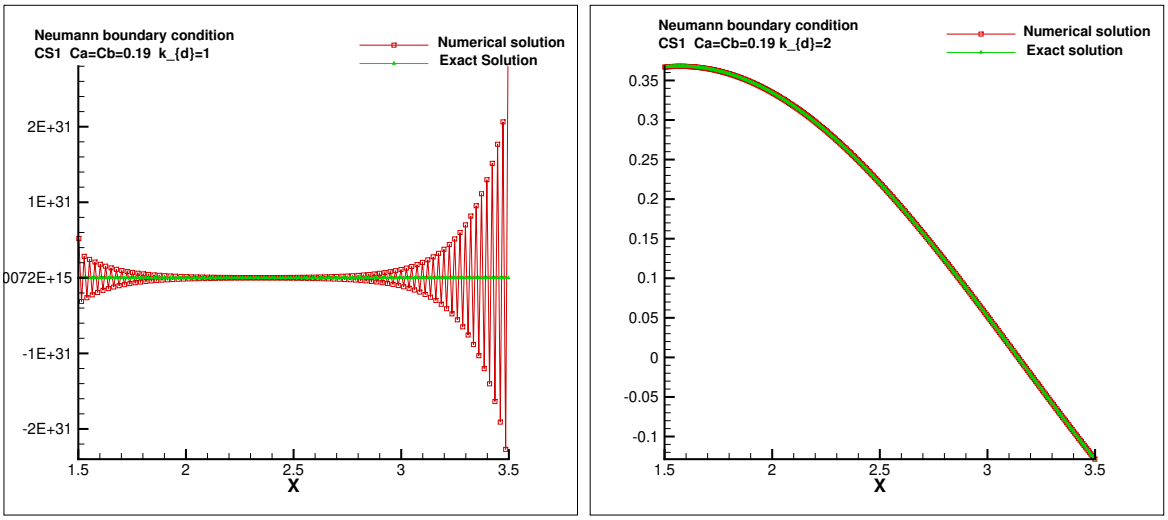

FIG. 4.20. The sixth order scheme CS1 and SILW procedure with $m = 6$, $C_a = C_b = 0.19$, $t_{end} = 1.0$. The CFL condition is in (4.32). Left: $k_d = 1$ and $N = 160$; Right: $k_d = 2$ and $N = 320$.

specifically, we use $\{(x_0, u_0), (x_1, u_1), \cdots, (x_8, u_8)\}$ and $\{(x_{n-8}, u_{n-8}), (x_{n-7}, u_{n-7}), \cdots, (x_n, u_n)\}$, that is, $m = 9$ as an example to get $P_{l,8}(x)$ and $P_{r,8}(x)$ which are polynomials of degree 8, respectively. By using the previous stability analysis procedure, we have $(k_d)_{min} = 2$. From Table 4.10, a grid refinement study verifies the designed sixth order accuracy.

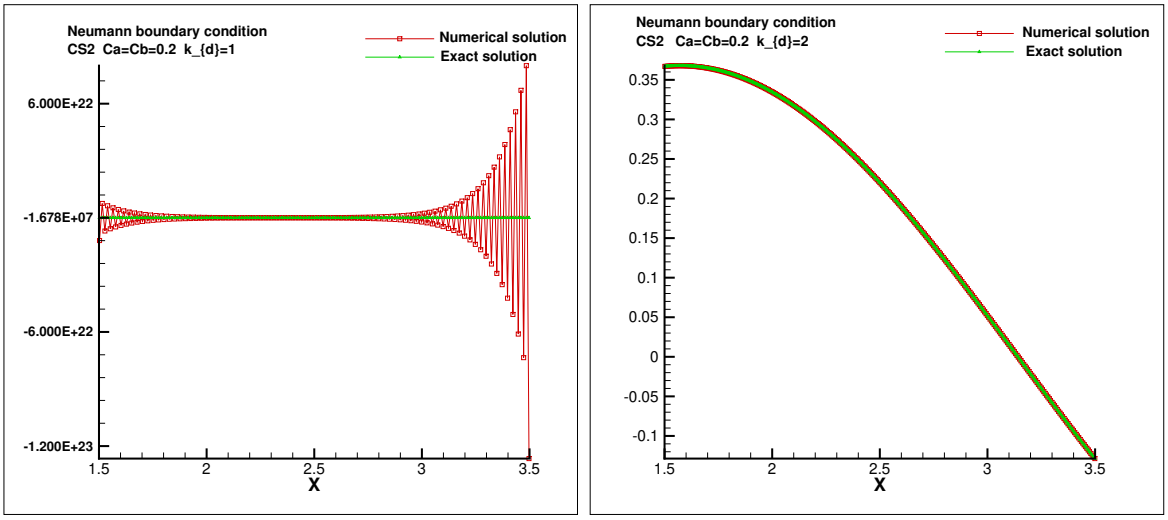

FIG. 4.21. The sixth order scheme CS2 and SILW procedure with $m = 6$, $C_a = C_b = 0.2$, $t_{end} = 1.0$. The CFL condition is in (4.32). Left: $k_d = 1$ and $N = 160$; Right: $k_d = 2$ and $N = 320$.

- The eighth order scheme CE1

We take $m = 2$ and in this case, the minimum value of k_d is 2. Fig. 4.22 shows the stability and instability results which is consistent with the analysis.

TABLE 4.9. The Sixth order scheme CS2 with $m = 6$, $k_d = 2$, $t_{end} = 1.0$ for the heat equation (4.29) with Neumann boundary conditions (4.31). The CFL condition is in (4.32).

N	$C_a = 10^{-8}$, $C_b = 10^{-8}$				$C_a = 1 - 10^{-8}$, $C_b = 1 - 10^{-8}$			
	L^2 *error*	order	L^∞ *error*	order	L^2 *error*	order	L^∞ *error*	order
10	4.912E-08	–	5.548E-08	–	5.078E-04	–	7.897E-04	–
20	5.917E-10	6.375	6.634E-10	6.386	4.932E-05	3.364	7.869E-05	3.327
40	8.141E-12	6.184	9.070E-12	6.193	3.886E-06	3.666	6.204E-06	3.665
80	1.197E-13	6.087	1.333E-13	6.089	2.732E-07	3.830	4.344E-07	3.836
160	1.795E-15	6.060	1.993E-15	6.064	1.805E-08	3.920	2.860E-08	3.925

TABLE 4.10. The Sixth order scheme CS2 with $m = 9$, $k_d = 2$, $t_{end} = 1.0$ for the heat equation (4.29) with Neumann boundary conditions (4.31). The CFL condition is in (4.32).

N	$C_a = 10^{-8}$, $C_b = 10^{-8}$				$C_a = 1 - 10^{-8}$, $C_b = 1 - 10^{-8}$			
	L^2 *error*	order	L^∞ *error*	order	L^2 *error*	order	L^∞ *error*	order
10	1.907E-07	–	2.231E-07	–	4.125E-04	–	5.872E-04	–
20	7.563E-10	7.978	8.129E-10	8.101	1.211E-05	5.090	1.955E-05	4.909
40	1.016E-11	6.217	1.069E-11	6.249	2.654E-07	5.512	4.323E-07	5.499
80	1.830E-13	5.796	1.734E-13	5.945	4.927E-09	5.751	7.934E-09	5.768
160	2.948E-15	5.955	2.731E-15	5.989	8.370E-11	5.879	1.331E-10	5.897

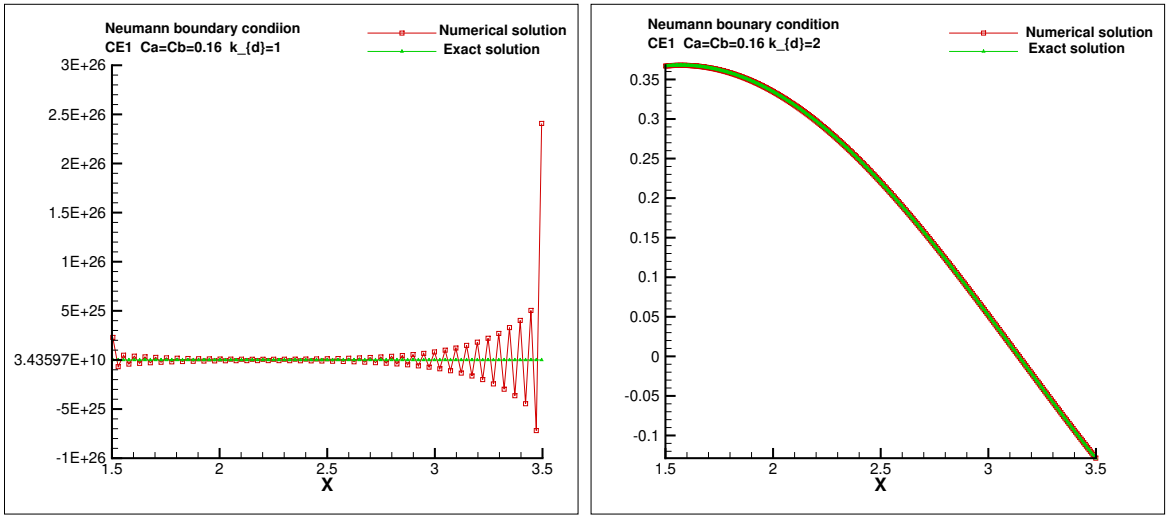

FIG. 4.22. The eighth order Scheme CE1 and SILW procedure with $m = 2$, $C_a = C_b = 0.16$, $t_{end} = 1.0$. The CFL condition is in (4.32). Left: $k_d = 1$ and $N = 80$; Right: $k_d = 2$ and $N = 320$.

• The eighth order scheme CE2

We take $m = 2$ and in this case, the minimum value of k_d is 3. Fig. 4.23 shows the stability and instability results which is consistent with the analysis.

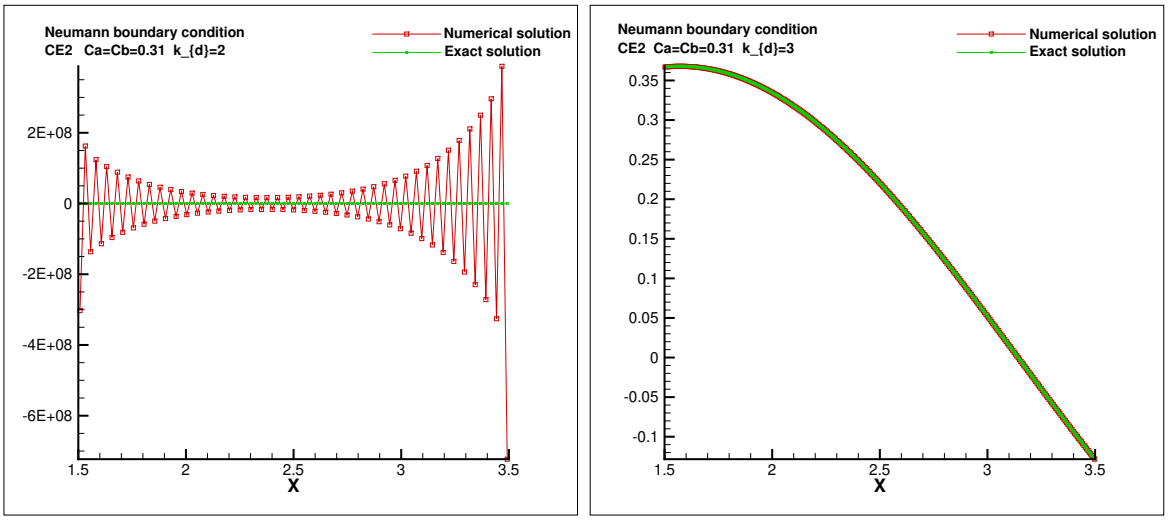

FIG. 4.23. The eighth order scheme CE2 and SILW procedure with $m = 2$, $C_a = C_b = 0.31$, $t_{end} = 1.0$. The CFL condition is in (4.32). Left: $k_d = 2$ and $N = 80$; Right: $k_d = 3$ and $N = 320$.

• The eighth order scheme CE3

We take $m = 8$ and the minimum value of k_d is 2. Fig. 4.24 shows the stability and instability results which is consistent with the analysis.

To match the order of accuracy, we take

$$\Delta t = (\lambda_{cfl})_{max} \Delta x^{\frac{8}{3}}. \tag{4.33}$$

Similar to the sixth order scheme CS2, results of grid refinements in Table 4.11 shows that we can only get the sixth order when C_a and C_b is large. In order to get the eighth order accuracy, we can use $\{(x_0, u_0), \cdots, (x_{10}, u_{10})\}$ and $\{(x_{n-10}, u_{n-10}), \cdots, (x_n, u_n)\}$, that is, $m = 11$ to get $P_{l,10}(x)$ and $P_{r,10}(x)$ which are polynomials of degree 10. In this case, $(k_d)_{min} = 2$ and then we can get the designed eighth order as shown in Table 4.12.

TABLE 4.11. The eighth order scheme CE3 with $m = 8$, $k_d = 2$, $t_{end} = 1.0$ for the heat equation (4.29) with Neumann boundary conditions (4.31). The CFL condition is in (4.33).

N	$C_a = 10^{-8}$, $C_b = 10^{-8}$				$C_a = 1 - 10^{-8}$, $C_b = 1 - 10^{-8}$			
	L^2 *error*	order	L^∞ *error*	order	L^2 *error*	order	L^∞ *error*	order
30	6.420E-13	–	6.056E-13	–	5.045E-08	–	8.160E-08	–
40	6.499E-14	7.962	6.036E-14	8.015	1.004E-08	5.611	1.621E-08	5.618
50	1.097E-14	7.973	1.009E-14	8.015	2.817E-09	5.697	4.537E-09	5.708
60	2.558E-15	7.986	2.340E-15	8.017	9.869E-10	5.752	1.586E-09	5.764
70	7.430E-16	8.019	6.786E-16	8.030	4.042E-10	5.790	6.486E-10	5.802

• The tenth order scheme CT1

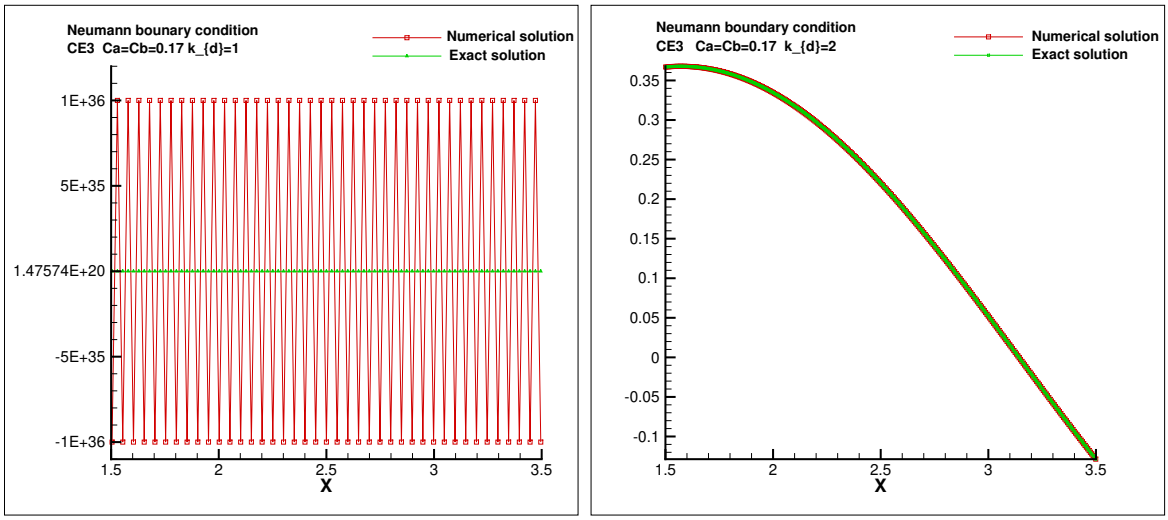

FIG. 4.24. The eighth order scheme CE3 and SILW procedure with $m = 8$, $C_a = C_b = 0.17$, $t_{end} = 1.0$. The CFL condition is in (4.32). Left: $k_d = 1$ and $N = 80$; Right: $k_d = 2$ and $N = 320$.

TABLE 4.12. The eighth order scheme CE3 with $m = 11$, $k_d = 2$, $t_{end} = 1.0$ for the heat equation (4.29) with Neumann boundary conditions (4.31). The CFL condition is in (4.33).

N	$C_a = 10^{-8}$, $C_b = 10^{-8}$				$C_a = 1 - 10^{-8}$, $C_b = 1 - 10^{-8}$			
	L^2 *error*	order	L^∞ *error*	order	L^2 *error*	order	L^∞ *error*	order
50	6.025E-15	–	5.164E-15	–	2.004E-11	–	3.284E-11	–
60	1.362E-15	8.154	1.193E-15	8.034	4.947E-12	7.672	8.086E-12	7.687
70	3.860E-16	8.181	3.424E-16	8.099	1.504E-12	7.723	2.452E-12	7.740
80	1.256E-16	8.406	1.123E-16	8.350	5.337E-13	7.760	8.680E-13	7.778
90	4.202E-17	9.299	3.767E-17	9.274	2.133E-13	7.788	3.461E-13	7.806

We take $m = 3$ and in this case, the minimum value of k_d is 3. Fig. 4.25 shows the stability and instability results which is consistent with the analysis.

• The tenth order scheme CT2

We take $m = 10$ and in this case, the minimum value of k_d is 3. Fig. 4.26 shows the stability and instability results which is consistent with the analysis.

• The tenth order scheme CT3

We take $m = 6$ and in this case, the minimum value of k_d is 4. Fig. 4.27 shows the stability and instability results which is consistent with the analysis.

• The tenth order scheme CT4

We take $m = 10$ and in this case, the minimum value of k_d is 4. Fig. 4.28 shows the stability and instability results which is consistent with the analysis.

• The tenth order scheme CT5

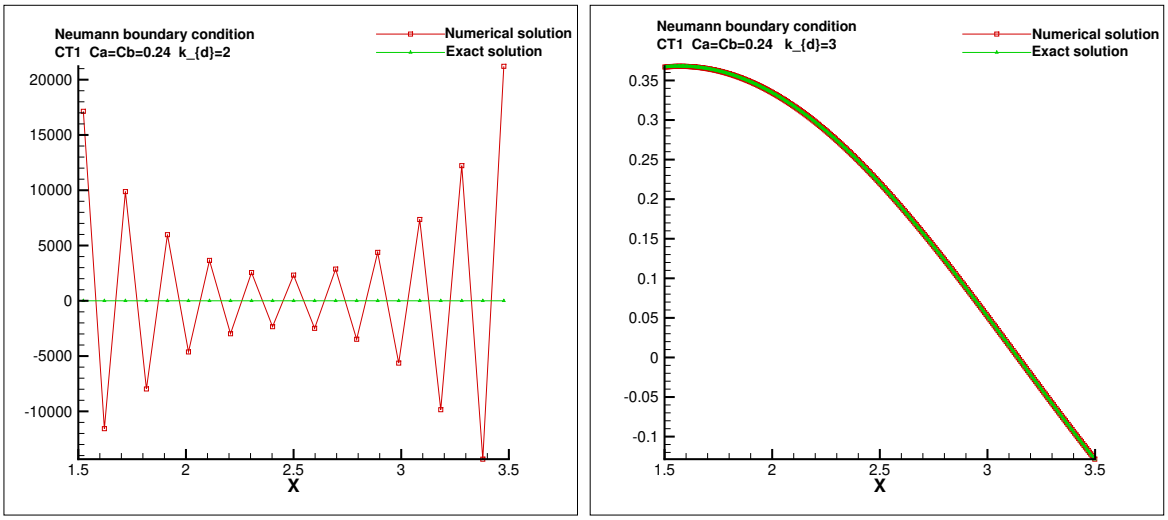

FIG. 4.25. The tenth order scheme CT1 and SILW procedure with $m = 3$, $C_a = C_b = 0.24$, $t_{end} = 1.0$. The CFL condition is in (4.32). Left: $k_d = 2$ and $N = 20$; Right: $k_d = 3$ and $N = 320$.

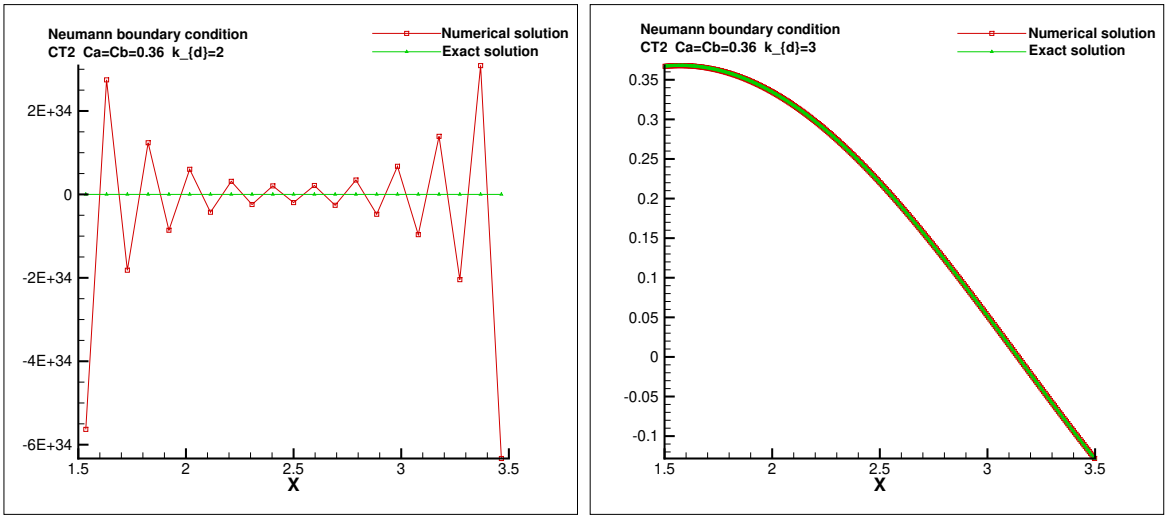

FIG. 4.26. The tenth order scheme CT2 and SILW procedure with $m = 10$, $C_a = C_b = 0.36$, $t_{end} = 1.0$. The CFL condition is in (4.32). Left: $k_d = 2$ and $N = 20$; Right: $k_d = 3$ and $N = 320$.

We take $m = 2$ and in this case, the minimum value of k_d is 3. Fig. 4.29 shows the stability and instability results which is consistent with the analysis. Similar to the case of the sixth order scheme CS2 and the eighth order scheme CE3, if we take

$$\Delta t = (\lambda_{cfl})_{max} \Delta x^{\frac{10}{3}} \tag{4.34}$$

we can only get the eighth order when C_a and C_b is large shown in Table 4.13. We use $\{(x_0, u_0), \cdots, (x_{11}, u_{11}), (x_0, (u_{xx})_0)\}$ and $\{(x_{n-11}, u_{n-11}), (x_{n-10}, u_{n-10}), \cdots, (x_n, u_n), (x_n, (u_{xx})_n)\}$, that is, $m = 12$ to get the interpolation polynomials $P_{l,12}(x)$ and $P_{r,12}(x)$

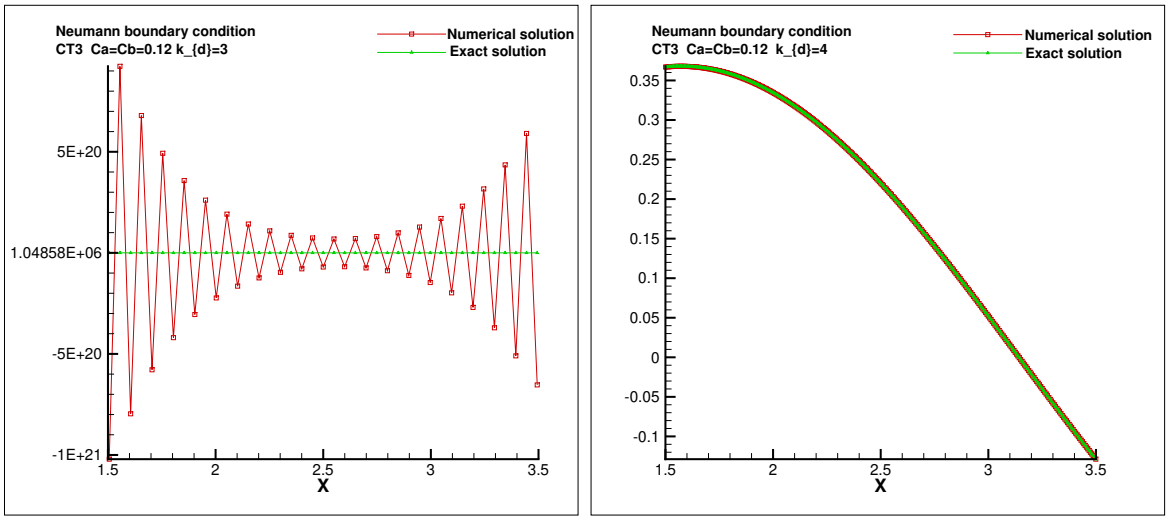

FIG. 4.27. The tenth order scheme CT3 and SILW procedure with $m = 6$, $C_a = C_b = 0.12$, $t_{end} = 1.0$. The CFL condition is in (4.32). Left: $k_d = 3$ and $N = 40$; Right: $k_d = 4$ and $N = 320$.

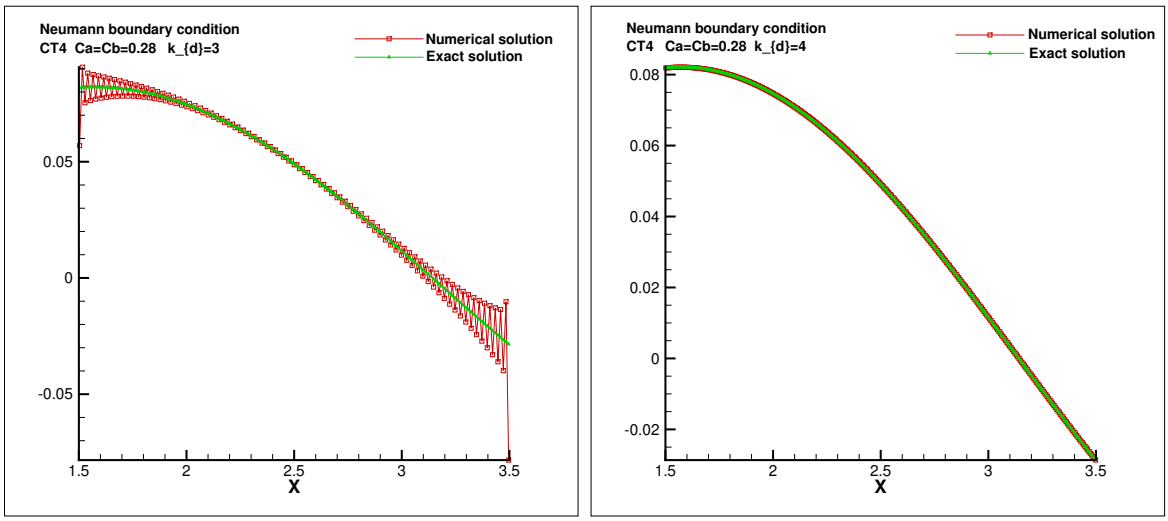

FIG. 4.28. The tenth order scheme CT4 and SILW procedure with $m = 10$, $C_a = C_b = 0.28$, $t_{end} = 1.0$. The CFL condition is in (4.32). Left: $k_d = 3$ and $N = 160$; Right: $k_d = 4$ and $N = 320$.

which are polynomials of degree 12. In this case, the minimum value of k_d is $(k_d)_{min} = 4$, then we can get the designed tenth order of accuracy as shown in Table 4.14.

5. Concluding Remarks

In this paper, we study the stability of the numerical boundary treatments for the high order compact finite difference schemes for solving parabolic equations with both Dirichlet and Neumann boundary conditions on a finite domain. We use the simplified inverse Lax-Wendroff (SILW) procedure to evaluate the ghost points and then get the numerical

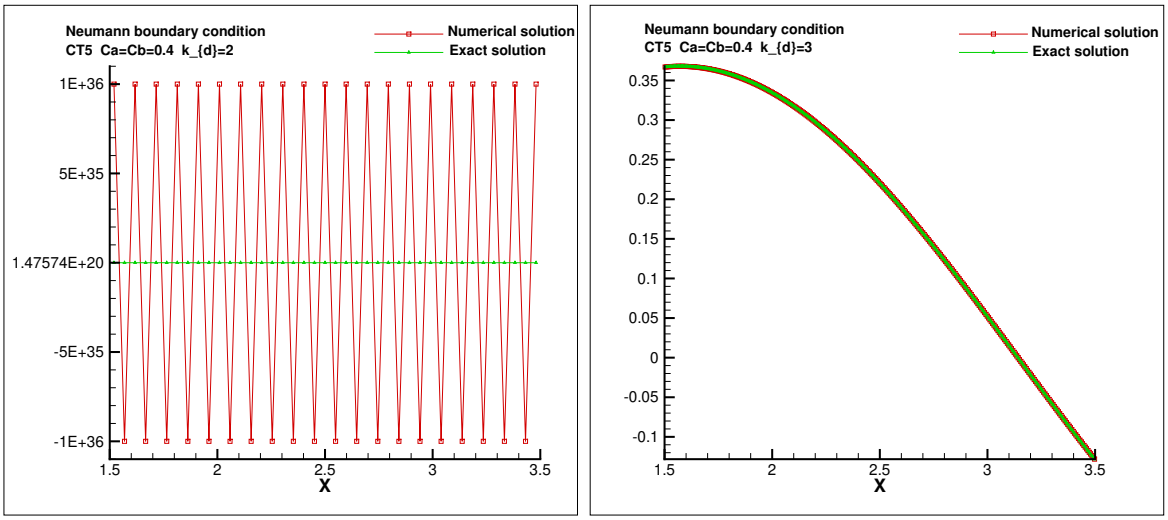

FIG. 4.29. The tenth order scheme CT5 and SILW procedure with $m = 2$, $C_a = C_b = 0.4$, $t_{end} = 1.0$. The CFL condition is in (4.32). Left: $k_d = 2$ and $N = 40$; Right: $k_d = 3$ and $N = 320$.

TABLE 4.13. The tenth order scheme CT5 with $m = 2$, $k_d = 3$, $t_{end} = 1.0$ for the heat equation (4.29) with Neumann boundary conditions (4.31). The CFL condition is in (4.34).

N	$C_a = 10^{-8},\ C_b = 10^{-8}$				$C_a = 1 - 10^{-8},\ C_b = 1 - 10^{-8}$			
	L^2 *error*	order	L^∞ *error*	order	L^2 *error*	order	L^∞ *error*	order
30	2.413E-15	–	2.176E-15	–	2.343E-10	–	3.818E-10	–
40	1.385E-16	9.933	1.236E-16	9.970	2.713E-11	7.494	4.415E-11	7.499
50	1.503E-17	9.952	1.333E-17	9.983	4.970E-12	7.606	8.065E-12	7.618
60	2.444E-18	9.963	2.156E-18	9.989	1.226E-12	7.677	1.984E-12	7.692
70	5.256E-19	9.970	4.621E-19	9.993	3.725E-13	7.727	6.016E-13	7.742

TABLE 4.14. The tenth order scheme CT5 with $m = 12$, $k_d = 4$, $t_{end} = 1.0$ for the heat equation (4.29) with Neumann boundary conditions (4.31). The CFL condition is in (4.34).

N	$C_a = 10^{-8},\ C_b = 10^{-8}$				$C_a = 1 - 10^{-8},\ C_b = 1 - 10^{-8}$			
	L^2 *error*	order	L^∞ *error*	order	L^2 *error*	order	L^∞ *error*	order
40	7.650E-17	–	6.965E-17	–	7.662E-14	–	1.256E-13	–
50	8.197E-18	10.010	7.479E-18	10.000	9.171E-15	9.513	1.500E-14	9.524
60	1.322E-18	10.008	1.208E-18	10.000	1.593E-15	9.601	2.598E-15	9.617
70	2.826E-19	10.007	2.586E-19	10.000	3.593E-16	9.662	5.842E-16	9.680
80	7.429E-20	10.007	6.803E-20	10.000	9.829E-17	9.707	1.594E-16	9.726

boundary conditions. Stability analysis is performed by both the Godunov-Ryabenkii analysis and the eigenvalue spectrum visualization method to get the pair $(m, (k_d)_{min})$ for the sake of stability, where m is the number of function values in constructing the

interpolation polynomial and k_d is the number of terms using the inverse Lax-Wendroff procedure. All analyses are under the standard CFL condition for the corresponding periodic problems. Numerical examples are provided to verify stability and instability results predicted by the analysis in Table 3.2 and 3.3. Currently we only consider the parabolic equation with Dirichlet or Neumann boundary conditions, however the Robin-type boundary condition is very challenging and the current approach cannot be applied to it easily. Therefore, to find a suitable numerical boundary treatment for Robin-type boundary condition will be one of our future works.

References

[1] M.J. Berger, C. Helzel and R.J. Leveque, *h-box methods for the approximation of hyperbolic conservation laws on irregular grids*, SIAM J. Numer. Anal. 41: 893–918, 2003.

[2] X.W. Bao, J. Yan and W.X. Sun, *A three dimensional tidal model in boundary-fitted curvilinear grids*, Coastal and Shelf Science, 50: 775–788, 2000.

[3] M.H. Carpenter, D. Gottlieb, S. Abarbanel and W.-S. Don, *The theoretical accuracy of Runge-Kutta time discretizations for the initial boundary value problem: a study of the boundary error*, SIAM J. Sci. Comput. 16: 1995, 1241–1252.

[4] S. Ding, C.-W. Shu and M. Zhang, *On the conservation of finite difference WENO schemes in non-rectangular domains using the inverse Lax-Wendroff boundary treatments*, J. Comput. Phys. 415, 2020.

[5] B. Gustafsson, H.-O. Kreiss and A. Sundström, *Stability theory of difference approximations for mixed initial boundary value problem. II*, Math. Comp. 26: 649–686, 1972.

[6] B. Gustafsson, H.-O. Kreiss and J. Oliger, *Time-dependent problems and difference methods*, Wiley-Interscience, 1972.

[7] S.K. Godunov and V.S. Ryabenkii, *Spectral stability criteria for boundary-value problems for non-self-adjoint difference equations*, (Russian) Uspehi Mat. Nauk 18: 3–14, 1963.

[8] Y. Jiang, C.-W. Shu and M. Zhang, *Free-stream preserving finite difference schemes on curvilinear meshes*, Methods Appl. Anal. 21: 1–30, 2014.

[9] H.-O. Kreiss, *Stability theory for difference approximations of mixed initial boundary value problems. I*, Math. Comp. 27: 703–714, 1968.

[10] H.-O. Kreiss and N.A. Petersson, *A second order accurate embedded boundary method for the wave equation with Dirichlet data*, SIAM J. Sci. Comput. 27: 1141–1167, 2006.

[11] J. Lu, J. Fang, S. Tan,C.-W. Shu and M. Zhang, *Inverse Lax-Wendroff procedure for numerical boundary conditions of convection-diffusion equations*, J. Comput. Phys. 317: 276–300, 2016.

[12] J. Lu, C.-W. Shu, S. Tan and M. Zhang, *An inverse Lax-Wendroff procedure for hyperbolic conservation laws with changing wind direction on the boundary*, J. Comput. Phys. 426, 2021.

[13] T. Li, C.-W. Shu and M. Zhang, *Stability analysis of the inverse Lax-Wendroff boundary treatment for high order upwind-biased finite difference schemes*, J. Comput. Appl. Math. 299: 140–158, 2016.

[14] T. Li, C.-W. Shu and M. Zhang, *Stability Analysis of the Inverse Lax-Wendroff Boundary Treatment for High Order Central Difference Schemes for Diffusion Equations*, J. Sci. Comput. 70: 576–607, 2017.

[15] S. Osher, *Stability of difference approximations of dissipative type for mixed initial-boundary value problems*, Math. Comp. 23: 335–340, 1969.

[16] S. Osher, *Stability of parabolic difference approximations to certain mixed initial boundary value problems*, Math. Comp. 26: 13-39, 1972.

[17] S.A. Orszag, and M. Israeli, *Numerical simulation of viscous Incompressible Flows*, Annu. Rev. Fluid Mech. 6: 281–318, 1974.

[18] C.-W. Shu and S. Osher, *Efficient implementation of essentially non-oscillatory shock-capturing schemes*, J. Comput. Phys. 77: 439–471, 1988.

[19] J.C. Strikwerda, *Initial boundary value problems for the method of lines*, J. Comput. Phys. 34: 94-107, 1980.
[20] E. Sousa, *Stability analysis of difference methods for parabolic initial value problems*, Journal of Scientific Computing, 26: 45–66, 2006.
[21] B. Sjögreen and N.A. Petersson, *A Cartesian embedded boundary method for hyperbolic conservation laws*, Commun. Comput. Phys. 2: 1199–1219, 2007.
[22] S. Tan and C.-W. Shu, *Inverse Lax-Wendroff procedure for numerical boundary conditions of conservation laws*, J. Comput. Phys. 229: 8144–8166, 2010.
[23] S. Tan and C.-W. Shu, *A high order moving boundary treatment for compressible inviscid flows*, J. Comput. Phys. 230: 6023–6036, 2011.
[24] S. Tan, C. Wang, C.-W. Shu and J. Ning, *Efficient implementation of high order inverse Lax-Wendroff boundary treatment for conservation laws*, J. Comput. Phys. 231: 2510–2527, 2012.
[25] J.M. Varah, *Stability of difference approximations to the mixed initial boundary value problems for parabolic systems*, SIAM J. Numer. Anal. 8: 598–615, 1971.
[26] F. Vilar and C.-W. Shu, *Development and stability analysis of the inverse Lax-Wendroff boundary treatment for central compact schemes*, ESAIM Math. Model. Numer. Anal. 49: 39–67, 2015.

School of Mathematics and Statistics, Henan University, Kaifeng, Henan 475000, China.
Email address: E-mail: ltt1120@mail.ustc.edu.cn.

South China Research Center for Applied Mathematics and Interdisciplinary Studies, South China Normal University, Canton, Guangdong 510631, China.
Email address: E-mail: jflu@m.scnu.edu.cn.

Division of Applied Mathematics, Brown University, Providence, RI 02912, USA
Email address: chi-wang_shu@brown.edu